DIAGNOSIS OF BREAST CANCER USING AUTO-FLOURESCENCE LIFETIME AND LIGHT REFLECTANCE SPECTROSCOPY: A POTENTIAL TOOL FOR POSITIVE MARGIN ASSESSMENT

By

SHIVARANJANI SHIVALINGAIAH

Submitted to the Office of Graduate Studies of

University of Texas at Arlington

in partial fulfillment of the requirements for the degree of

MASTER OF SCIENCE IN BIOMEDICAL ENGINEERING

University of Texas at Arlington

December 2011

ACKNOWLEDGEMENTS

Research is an ongoing process of embracing failure and triumph. However, in the words of Carl Sagan, *"Somewhere, something incredible is waiting to be known."* All the incredible things I was exposed to were made possible by some of the most inspiring researchers that I have come across during my years of graduated studies. I would like to thank all the people who have helped and inspired me throughout this process.

I owe my deepest gratitude to my Graduate advisor, Dr.Hanli Liu, for her guidance and words of encouragement during my research and study. She is a woman of perpetual energy and enthusiasm, motivating all her advisees. She has always been accessible and willing to help her students giving us an opportunity to hone our researching abilities.

I am highly indebted to my professors Dr.Samarendra Mohanty, Dr.George Alexandrakis, Dr. Peng and Dr. Karel Zuzak, for guiding me by example, through challenging coursework on how to think, apply and never give up in my quest for scientific pursuits. I would like to thank Dr. David Euhus for providing us with invaluable specimens and Dr.Peng for histological analysis. I once again thank them for accepting to be on my dissertation committee.

I am also very thankful to Vikrant Sharma and Nimit Patel for their patience, research support and encouragement through the course of my thesis. Lastly, I extend my gratitude all my friends and family for their unflagging love and support throughout this endeavor.

November 9, 2011

ABSTRACT

DIAGNOSIS OF BREAST CANCER USING AUTO-FLOURESCENCE LIFETIME AND LIGHT REFLECTANCE SPECTROSCOPY: A POTENTIAL TOOL FOR POSITIVE MARGIN ASSESSMENT

Shivaranjani Shivalingaiah, M.S

The University of Texas at Arlington

and

The University of Texas Southwestern Medical Center at Dallas, 2011

Supervising Professor: Dr.Hanli Liu

Malignant Breast Neoplasm (MBN) or breast cancer is a heterogeneous cancer type originating in the breast tissue. Surgery is considered the primary treatment for breast cancer, with many early stage patients being cured without recurrence. The goals of the surgery include complete resection of the primary tumor, with negative margins to reduce the risk of local recurrences. Further, pathological staging of the tumor and axillary lymph nodes are carried out to extract necessary prognostic information.

Surgery works well in case of complete Mastectomies. However, the biggest challenge for this technique is determining adequate margins on the partial mastectomy (lumpectomy) specimen. In 30-50% of patients, positive margins are reported, resulting in additional surgery, leading to potential hazards like reduction in breast size, higher risk of wound infection and loss of

confidence in the surgical procedure. Therefore, there exists a high demand for investigating into mechanisms that will potentially aid in reducing the rate of positive margins and thereby reducing the case for re-excision Optical techniques can play an important role in diagnostics, breast cancer evaluation and treatment. This thesis outlines the possibility of combining two powerful modalities and extracting parameters that offer better diagnosis and margin assessment. Clinical post-operative readings were obtained from excised breast samples, using by auto-fluorescence life-time measurement (AFLM) and the light reflectance spectroscopy (LRS). Specifically, Seven breast cancer specimen, histopathologicaly diagnosed as Invasive Ductal Carcinoma with no history of pre-surgical chemotherapy, were investigated using dual optical modalities to derive statistical differences between breast cancer (i.e. IDC) and normal breast tissue (i.e. ductal epithelium)**.** The results demonstrate that both AFLM derived and LRS-derived parameters can serve as biomarkers in differentiating tumor from normal tissue in human breast. Specifically, spectral slopes at four wavelength regions in LRS have shown significant differences between cancer and normal tissues; a classification algorithm was further used to generate a receiver operating characteristic (ROC) curve determining the capability of LRS as a possible diagnostic tool for breast tissue for malignancy.

TABLE OF CONTENTS

LIST OF ILLUSTRATIONS

Figure Page

LIST OF TABLES

Table Page

CHAPTER 1

INTRODUCTION

In 1929, the first attempt in utilizing light for imaging the breast tissue was reported by Cutler et al [1]. This optical projection imaging was carried out by trans-illuminating the breast sample in a dark room and visually looking for shadows cast by large breast tumors. Several developments over the years have led to renewed interest in optical imaging of the breast, notably the improvements in photon migration theory, advancements in light sources and detectors, and enhanced numerical modeling techniques coupled with computing power to name a few. Further improvements in diagnostic information can be achieved by using optical methods in imaging of the tissue samples.

Although there are several optical techniques that can be employed for breast cancer diagnosis, this thesis outlines the use of two imaging modalities namely, Auto-Fluorescence Lifetime Measurement (AFLM) and Light Reflectance Spectroscopy (LRS) in unison. Using the key features extracted from the fluorescence and reflectance spectra, a diagnostic algorithm for differentiation of normal from malignant breast tissue is obtained. In combination, these techniques provide a better understanding of biochemical and/or morphological changes that take place in the presence of malignant cells in the breast tissue. The overall goal of this research project was to develop fluorescence and reflectance spectroscopy as a diagnostic tool for detection, differentiation of breast cancers and assessment of positive breast margins to guide breast conserving surgery.

Breast Cancer is the most common form of cancer in females and accounts for the highest number of fatalities in women, only after lung cancer. It is a form of malignancy originating in the cells of the breast tissue. An extensive understanding of breast pathology and morphologic changes associated with breast cancer is imperative, in order to apply spectroscopy for breast cancer diagnosis. This chapter details with fundamentals of Breast Cancer. Both breast anatomy and pathology are described, thereby providing a framework for interpretation of spectroscopic data. Current breast cancer diagnostic strategies as staging, prognosis and treatment are also summarized in this chapter.

1.1 Breast Anatomy

The mature breast serves as a secretory, milk producing gland [2]. Breast tissue extends from below the collarbone to the level of the sixth or seventh rib and extends from the breastbone to the axilla. The breast has no muscle tissue. A layer of fat surrounds the glands and extends throughout the breast. In the center of the breast are the nipple and the areola. The mammary glands, or milk producing areas, lie between the Pectoralis major muscle and the skin. The breast is responsive to a complex interplay of hormones that cause the tissue to develop, enlarge and produce milk. The three major hormones affecting the breast are estrogen, progesterone and prolactin, which cause glandular tissue in the breast and the uterus to change during the menstrual cycle.

The glands that make milk in the breast are arranged into rounded areas called lobules. 15-20 of these lobules exist per breast. A thick layer of subcutaneous adipose tissue covers the lobes and gives the breast its size and shape. Each lobe is comprised of many lobules, at the end of which are tiny bulb like glands, or sacs, where milk is produced in response to hormonal signals (see Fig. 1.1). Ducts connect the lobes, lobules, and glands in nursing mothers.

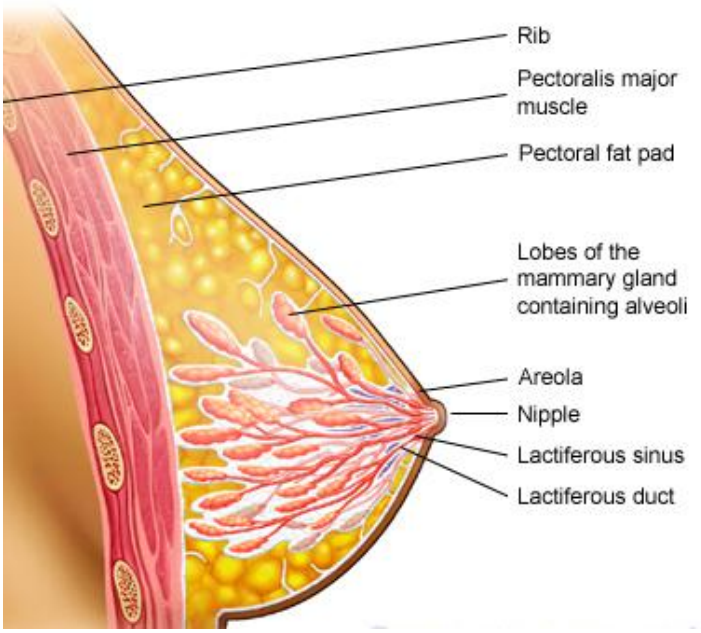

Fig 1.1: A schematic of the female breast. [53]

These ducts deliver milk to openings in the nipple. The areola is the darker-pigmented area around the nipple. Fibrous connective tissue, called fascia, lies between the breast tissue and the skin, separating it from the chest muscles. Coopers ligaments, which are made of elastin, run deep through the fascia, attaching firmly to the dermis, to provide a supportive network for the breast.

The internal mammary, axillary and intercostals veins drain the de-oxygenated blood out of the breast. The surface veins' encircling the nipple directs blood to internal mammary, axillary and intercostals veins and the lungs. Breast cancer can travel to the lungs via surface veins to result in metastatic tumors. Breast cancer cells can also spread to the bone tissue considering the intercostals veins of the breast joining into a complex network of vertebral veins around the spine.

Lymphatic vessels present in the breast, drain fluids into a network of lymph nodes located around the edges of the breast, in the underarm and the collarbone. Therefore, axillary lymph nodes are the first site of metastasis of malignant cells.

1.1.1 Normal Breast Tissue

The breast tissue is primarily comprised of three main tissue types; adipose, fibrous and glandular tissues [3]. Fatty or the adipose tissue interspersed with fibrous or the connective tissue makes up the stroma that is lying between the glands. The adipose tissue is composed of adipocytes that harbor copious amount of cytoplasmic fat, while the fibrous tissue comprises mainly of collagen. The glandular tissue is made up by several lobes or milk glands connected by a conduit of ducts that direct it towards the nipple. Each lobe is autonomous and empties into its own excretory duct. Lobes are divided into smaller units called the lobules, which are in turn made of acini. The lobules are the functional milk producing units. The lobular units and the ducts are separated from the stroma by a basement membrane composed of collagen.

In Fig 1.2 (a), there can be identified a low flattened layer of contractile cells, some slightly vacuolated, present beneath the more prominent epithelial lining. The larger ducts are lined by double layer of cuboidal cells and an inner layer of epithelial cells surrounded by a layer of myoepithilial lining. In Fig 1.2 (b), Myoepithilial cells can be observed between the epithelium and the basement membrane, containing myofilaments. They orient parallel to the long axis of the duct, enabling them to control the transport of milk. As the ducts become smaller, they only have a single layer of epithelial cells.

During several stages of female development, hormonal influences due to menstruation, pregnancy and/or menopause, cause significant changes in the breast tissue.

In the first half of the menstrual cycle, the lobules are relatively quiescent. Once the ovulation begins, under the influence of estrogen and rising levels of progesterone, the number of acini per lobule increases and so does the cell proliferation. With the onset of menstruation, the fall in estrogen and progesterone levels is followed by apoptosis, programmed epithelial cell death.

During pregnancy, the female breast undergoes lobular hypertrophy, to enable lactation following birth [2]. By the end of the pregnancy, the breast is composed almost entirely of lobules, which secretes milk. The epithelial lining in the Fig 1.2 (b) shows apocrine secretion or cytoplasmic extrusions into the lumen. 15 to 20 ducts come together near the areola to form reservoirs of milk ready to be extracted from the nipple. After lactation ends, the lobules experience atrophy, resulting in diminishing of the breast size. Onset of menopause results in atrophy of ducts and lobules and the stroma which is largely collagen to be replaced by fat.

1.2 Breast Pathology

Changes in the breast may be result in either Benign (non-cancerous) or Malignant (cancerous) lesions.

1.2.1 Benign Breast Lesions

Fibrocystic change that manifests itself as Fibrosis (formation of fibrous tissue), Adenosis (increase in number of ductules) or Cyst formation (dilation of ducts and lobules with semi-transparent fluid) can be classified as benign breast lesions. Micro-calcifications are very small mineral deposits, calcified secretory material or necrotic debris, within the breast tissue.

Fibro-adenoma, a common benign tumor, is induced by estrogen and often stimulated by lactation and pregnancy [5]. The tumor is composed of fibroblastic stroma which comprises of elongated compressed ducts lined by benign appearing epithelium.

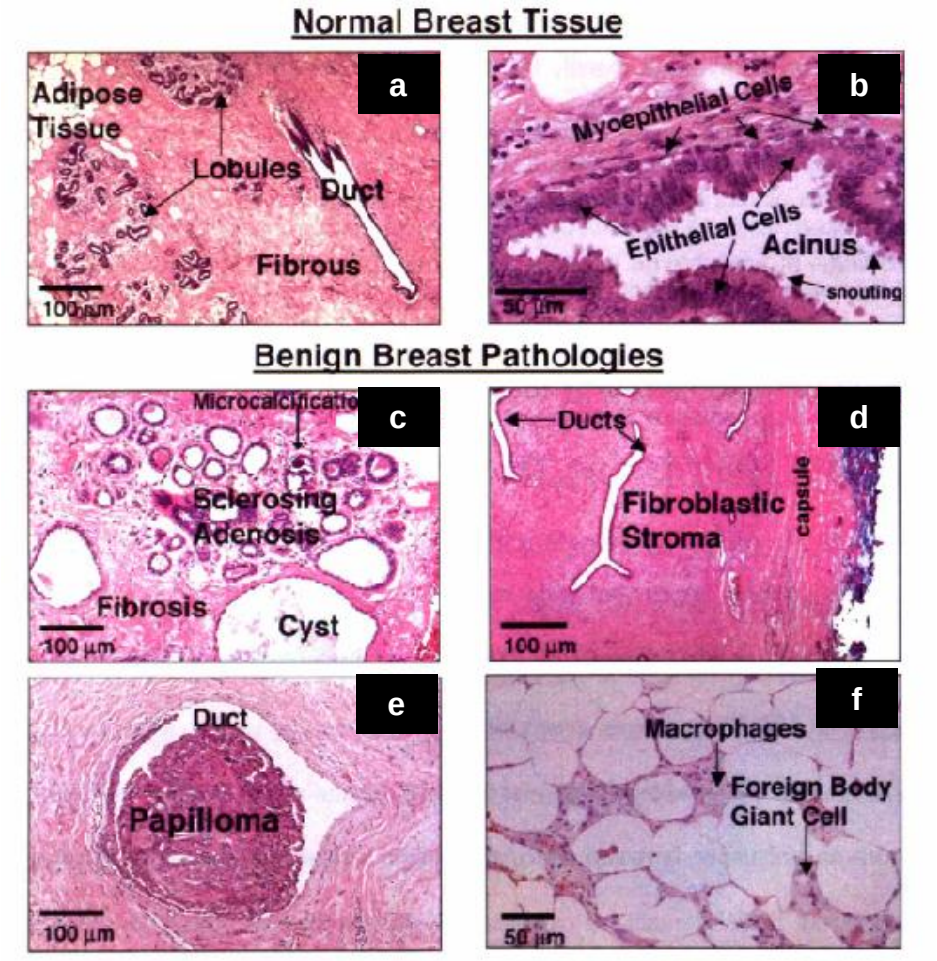

Fig 1.2: Haemotoxylin and Eosin staining of (a-b) Normal and (c-f) benign tissues [54]

Fibro-adenoma shows accumulation of collagen due to fibroblast proliferation resulting in expansion of stroma. Fat necrosis is another benign pathology descriptive of focal areas of fat destruction.

During histopathological observation, the tissue is fixed, sectioned, stained, visually examined by a pathologist and evaluated for abnormalities [4]. Hematoxylin and Eosin (H&E) is applied to tissues fixed in formalin.

Hematoxylin is a basic dye that stains acidic structures purplish blue, while Eosin, an acidic dye, stains basic structures red or pink. Fig 1.2 (a) - The three tissue types which make up the normal breast tissue can be observed here. Nuclei, ribosome and rough endoplasmic reticulum have high DNA and RNA content, and show a strong affinity towards Hematoxylin. Most cytoplasmic proteins are basic, and take up eosin. Fibrous tissues are also made up of basic proteins and hence stain pink or pinkish red. As seen in Fig 1.2 (a), purplish appearing ducts and lobules are lined with glandular epithelium. The epithelium appears purple due to abundance of cell nuclei. Adipose tissue can be observed as clear vacuolar spaces since fat is washed away during tissue processing. Fig 1.2 (b) depicts a magnification of normal breast acinus. A flattened layer of contractile cells, slightly vacuolated, can be observed beneath the epithelial lining. Inner layer of cells are surrounded by myoepithilial cells, in case of larger ducts. Snouting is the process of secretion of milk, by cytoplasmic extrusions into the lumen. Fig 1.2 (c) determines fibrocystic changes in the breast. Cystically dilated ducts and lobules are laced with excess fibrous connective tissue. Fig 1.2 (d) illustrates Fibroadenoma. Fig 1.2 (e) shows the presence of intraductal papilloma in the breast duct. Intraductal papilloma is a benign form of tumor arising from the ductal surface accompanied by serous or bloody nipple discharge. Fig 1.2 (f) shows fat necrosis at high magnification. Lipid laden macrophages can be observed between the necrotic adipose tissue cells.

1.2.2 Breast Cancer

Breast cancer is one of the most common forms of malignancy in women. It continues to be a major burden and cause of death among women worldwide. A malignant tumor consists of a group of abnormal cells that have developed from the stem cells of the breast and as time progresses, may invade other regions of the body.

Genetic mutations hamper the normal cell signaling system allowing cellular proliferation and growth to occur in the absence of external stimuli. They become resistant to apoptosis, thus dividing constantly and ultimately forming a tumor blob that is made up of billions of copies of original cancerous cells [6].

The earliest form of breast cancer, Ductal Carcinoma in-situ (DCIS) develops inside the milk ducts. The term *in situ* refers to cancer that has not spread past the area where it initially developed. Although it is non-invasive, Fig 1.3 (a), it is still considered malignant as it can develop into invasive cancer when it spreads outside the milk duct.

The most common and aggressive form of breast cancer, Invasive Ductal Carcinoma (IDC) as shown in Fig 1.3 (b), develops from DCIS, spreading through the duct walls and invading the surrounding breast tissue. 80% of all the invasive breast cancers accounts for IDC [2]. Lobular Carcinoma in-situ (LCIS) consists of neoplastic cells proliferating in the ducts and the acini of the breast. These cells are small with oval or round nuclei. Fig 1.3 (c) depict LCIS. Presence of LCIS increases the risk of developing Invasive Lobular Carcinoma by 30%. Invasive (Infiltrating) Lobular Carcinoma (ILC) comprises of malignant neoplastic cells that have spread outside of the breast lobules and spread to the other parts of the breast [2, 7]. Fig 1.3 (d) depicts the diffusely invasive pattern of ILC.

Inflammatory Breast Cancer (IBC) is caused by metastatic cells blocking the lymph vessels (Fig 1.3 (e); prominent lymphatic spaces can be filled by breast carcinoma, and can be seen on the skin overlying the breast. The skin turns red and has a pitted appearance. The early stages of IBC can be mistaken for an infection since the effect of IBC on the breast is similar to an infection [7]. IBC has a very high risk of spreading to the other parts or organs of the body and it

only accounts for about 1% to 3% of all the invasive breast cancers. Inflammatory carcinoma tends to spread quickly.

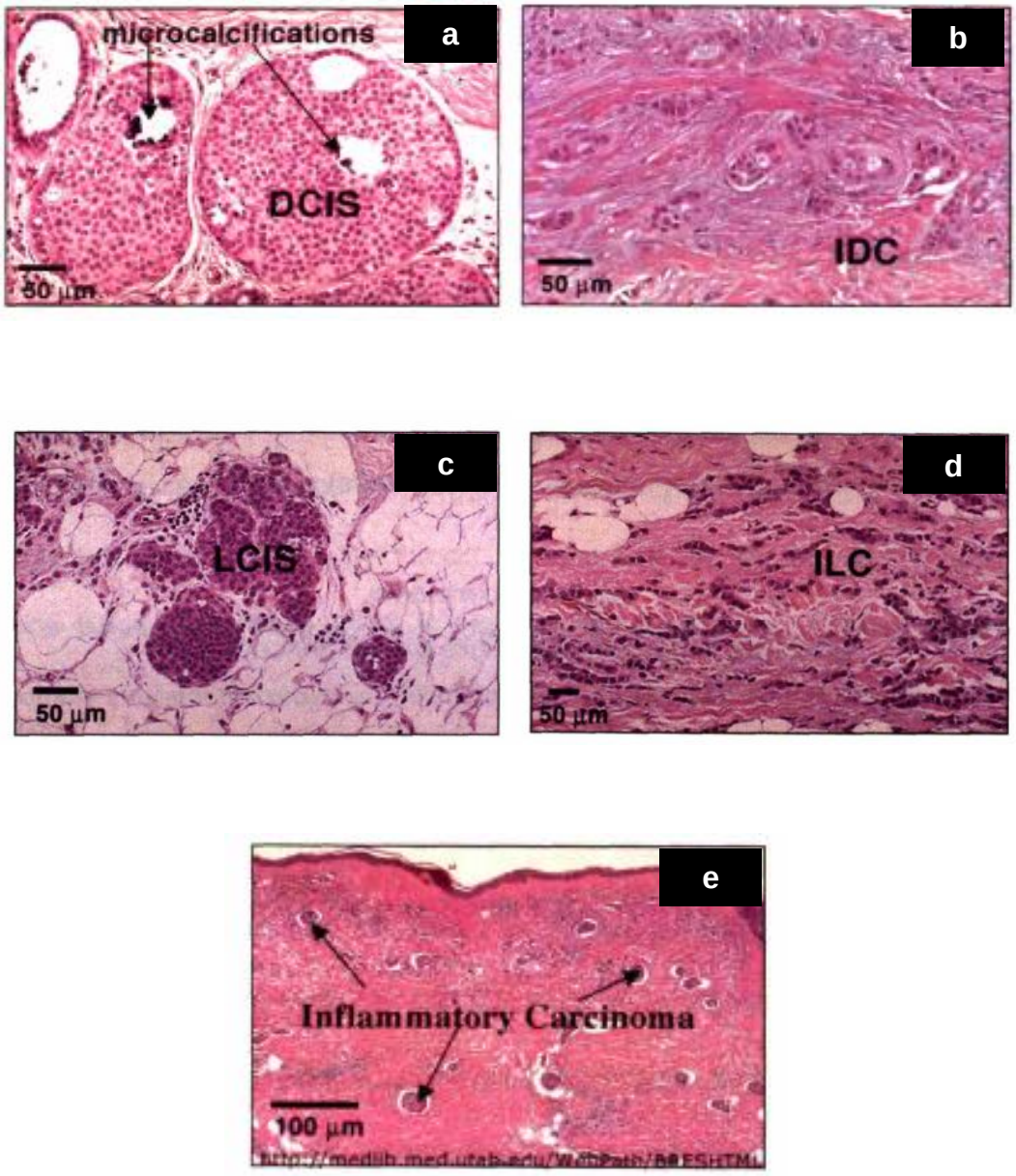

Fig 1.3: Illustrates H&E stained microscopic view of (a) DCIS, (b) IDC, (c) LCIS, (d) ILC and (e) IBC type of invasive cancer. [54]

1.3 Breast Cancer Risk Factors

A risk factor is any factor that affects a person's chance of contracting a disease, such as cancer. There exist several risk factors for breast cancer. These include female gender, age, prior occurrence of breast cancer, benign breast disease, hereditary factors (family history of breast cancer), early age of menarche, late onset of menopause, late onset of first full-term pregnancy, post-menopausal obesity, low physical activity, race/ethnicity and high-dose exposure to ionizing radiation early in life [10-13].

Furthermore, there are "speculated" risk factors for breast cancer that include never having been pregnant, having only one pregnancy rather than many, not breast feeding after pregnancy, use of postmenopausal estrogen replacement therapy or postmenopausal hormone (estrogen/progestin) replacement therapy, use of oral contraceptives, certain specific dietary practices (high intake of fat and low intakes of fiber, fruits, and vegetables, low intake of phytoestrogens), alcohol consumption, tobacco smoking, and abortion[14].

Although men can and do develop breast cancer [10], the disease is 100 times more likely to occur in a woman than in a man, since woman have much more breast tissue than men do. Also, estrogen promotes the development of breast cancer. The risk of breast cancer is higher in middle-aged and elderly women than in young women [11]. Epidemiological studies have shown that in women with a family history of breast cancer, the risk of breast cancer is increased two- to threefold [15]. Studies have also shown that there are families in which breast cancer risk is inherited in an autosomal-dominant fashion ('hereditary breast cancer').

Further, women who reach menarche at a relatively young age (12 or younger) and those who reach menopause at a relatively older age (55 or older) are slightly more likely than other

women to develop breast cancer. These relationships are believed to be mediated through estrogen production [16]. During the reproductive years, a woman's body produces high levels of estrogen. Women who start to menstruate at an early age and/or reach menopause at a late age are exposed to high levels of estrogen for more years than the women who have a late menarche or early menopause.

Age at first pregnancy is another aspect of reproductive history that is associated with breast cancer risk. Women who have their first full-term pregnancy at a relatively early age have a lower risk of breast cancer than those who never have children or those who have their first child relatively late in life. The biologic basis for this relationship is not entirely clear. Obesity has been consistently associated with an increased risk of breast cancer among postmenopausal women. This relationship may be mediated again by estrogen production [17]. Fat cells produce some estrogen and obese postmenopausal women, therefore, tend to have higher blood estrogen levels than counterpart.

Women who were exposed to high doses of radiation, especially during adolescence, have an increased risk of breast cancer [18]. This association has been observed both among atomic bomb survivors and among women who received high-dose radiation for medical purposes. Parity (having children) and the age of the woman at the birth of her first offspring are other endogenous hormonal factors that influence breast cancer. Women who have never had children (nulliparous) are at greater risk for the development of breast cancer than women who have had children (parous). The long-term (more than five years) use of postmenopausal estrogen therapy (ERT) or combined estrogen/progestin hormone replacement therapy (HRT) may be associated with an increase in breast cancer risk.

A possible relationship between breast cancer and diet has been suggested. Diets high in fruits and vegetables and low in fat and calories are healthful for many reasons, and they may indirectly reduce the risk of breast cancer by helping to prevent obesity [19]. There is also some evidence that cigarette smoking may be associated with a small increase in breast cancer risk [20]. Among women who have already been diagnosed with breast cancer, smoking may be associated with an increased risk that the cancer will progress more rapidly [21].

1.4 Breast Cancer Screening

The American Cancer Society has put forth a set of guidelines to follow for early detection of Breast Cancer. Following are the screening guidelines for most adults.

- Women at age 20 should know how their breasts normally look and feel and report any changes promptly to their health care provider. Learning the benefits and limitations of Breast self-examination (BSE) are important too.
- Women aged between the 20s and 30s, must have their breast examined by a physician for every 3 years and once annually for women over 40.
- Yearly mammograms are recommended starting at age 40 and continuing for as long as the woman is in good health.
- Women with a family history of Breast Cancer are recommended to be screened with an MRI in addition to mammograms.

1.5 Breast Cancer Diagnosis

Breast cancer is usually diagnosed by the woman and then confirmed by the physician after putting the person through a triple assessment diagnostic procedure. The most common

symptom of breast cancer is a new lump or mass. It can be a painless, hard mass that has irregular edges or masses that are tender, soft and/or rounded. For this reason, it is important that any new breast mass or lump must be checked by a health care professional experienced in diagnosing breast diseases. Diagnosis of breast cancer involves following steps.

1.5.1 Clinical breast examination (CBE)

Clinical breast examination (CBE), also known as palpation, involves the heath-care physician palpating the breast to detect any possible masses inside the breast, looking for suspicious areas feeling their texture and size with respect to the skin around the chest muscles [22]. Any changes in the nipples or the skin of your breasts will be noted. The lymph nodes in the armpit and above the collarbones may be palpated (felt), because enlargement or firmness of these lymph nodes might indicate spread of breast cancer.CBE is highly dependent on the physician's skills, expertise and experience. Although the techniques for CBE are well established, its effectiveness is still dependent on how good the physician is. Therefore further confirmation is necessary.

1.5.2 Imaging Techniques

1.5.2.1 Mammogram

Mammography is the most common diagnostic imaging modality used for breast cancer diagnosis and it uses X-ray radiation [23]. It is most effective in detecting abnormalities in fatty tissue. It is not very useful for women under the age of 40 due to the high glandularity of their breasts. Imaging views often used for screening mammography are cranio-caudal (head-to-foot), sagittal and oblique (cranio-caudal view shifted to include axillary tail) views.

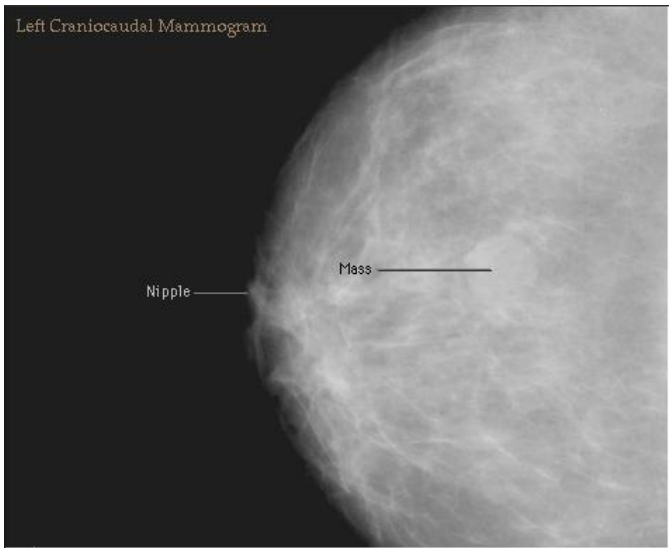

Fig 1.4: Breast mammogram [55]

A diagnostic mammogram can throw light upon:

- The severity of the abnormality in the breast.
- If the lesion (area of abnormal tissue) detected has a high probability of being benign (not cancer) or malignant.
- If the lesion is more suspicious, a biopsy is needed to confirm if it is cancer or not.

Even if the mammograms show no tumor, if you or your doctor can feel a lump, a biopsy is usually performed to make sure it isn't cancer [24]. One exception would be if an ultrasound exam finds that the lump is a simple cyst (a fluid-filled sac), which is very unlikely to be cancerous.

1.5.2.2 Breast Ultrasound

Breast Ultrasound is currently used as an adjuvant for X-ray mammography. Ultrasound uses sound waves to outline a part of the body. For this test, a small, a transducer is placed on the

skin (which is often first lubricated with ultrasound gel). It emits sound waves and picks up the echoes as they bounce off body tissues. The echoes are converted by a computer into a two-dimensional black and white image which is perpendicular to the plane where the transducer is placed and that image that is displayed on the computer screen. This test is painless and does not expose you to radiation [25].

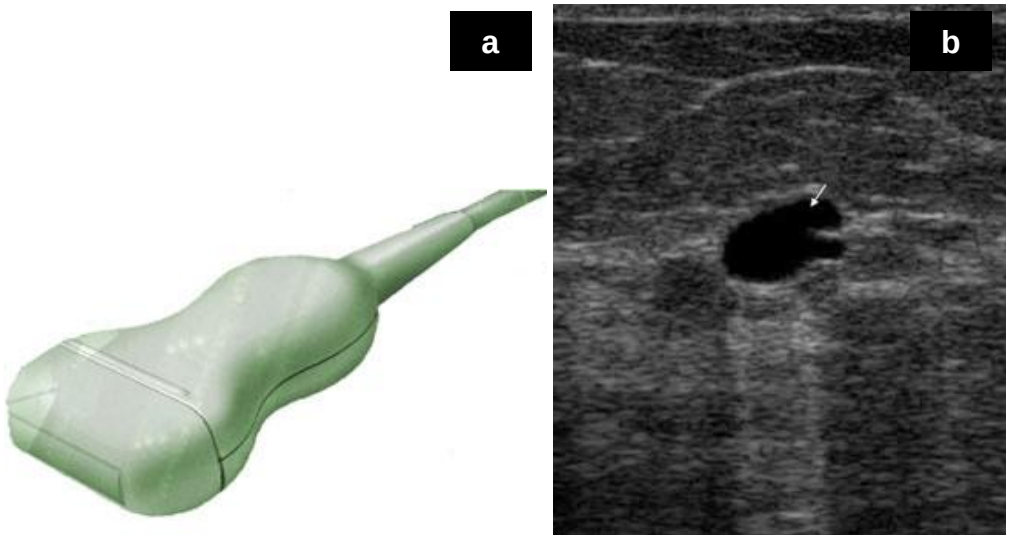

Fig 1.5: (a) Ultrasound probe [56] (b) Ultrasound image of a breast cyst. [57]

The use of ultrasound instead of mammograms for breast cancer screening is not recommended. Usually, breast ultrasound is used to target a specific area of concern found on the mammogram. Ultrasound helps distinguish between cysts (fluid-filled sacs) and solid masses and sometimes can help tell the difference between benign and cancerous tumors. Ultrasound may be most helpful in women with very dense breasts.

1.5.2.3 Magnetic Resonance Imaging (MRI)

1.5.2.3 Magnetic Resonance Imaging (MRI)

MRI scans uses radio waves and strong magnets in the place of x-rays. The energy from the radio waves is absorbed and bounced off by the body tissue in a specific pattern and changes in the presence of diseases [26, 27]. A computer translates the pattern into a very detailed image of parts of the body. For breast MRI to look for cancer, a contrast liquid called gadolinium is injected into a vein before or during the scan to show details better.

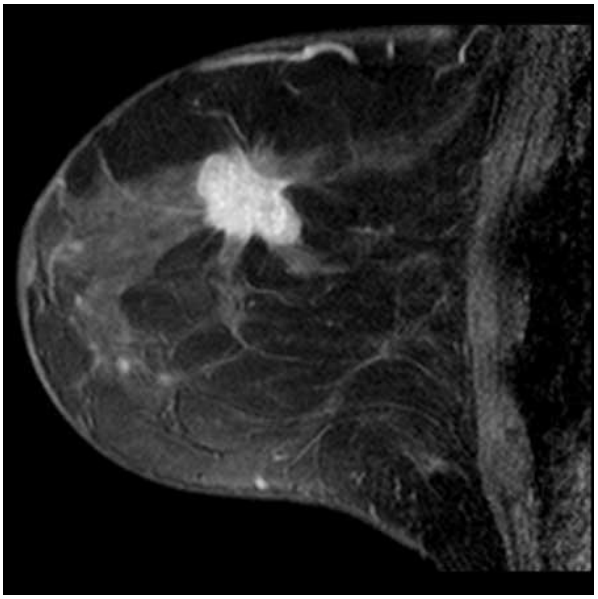

Fig 1.6: Breast MRI. [58]

MRI is still considered a research modality due to its high expense and low throughput. It has high sensitivity (true-positive rate), but low specificity (false-negative rate). It may be the most effective modality for Invasive lobular carcinoma (ILC) which is difficult to detect in mammography, and for women with breast implants. False-negative interpretations have been reported particularly for DCIS, due to occasional lack of tumor angiogenesis and poor

enhancement. Three-dimensional MRI images can be seen in sagittal, axial, or coronal views, depending on the application.

1.5.2.4 Ductogram

Ductogram helps determine the cause of nipple discharge. In this test a very thin plastic tube is placed into the opening of the duct in the nipple that the discharge is coming from. A small amount of contrast medium is injected, which outlines the shape of the duct on an x-ray image and shows if there is a mass inside the duct [28].

1.5.3 Biopsy

Biopsy refers to removal of tissue from patients for diagnostic examination. During biopsy, the surgeon removes a sample of the lesion to be examined under the microscope. A biopsy is performed when mammogram/other imaging tests, or the physical exam finds a breast abnormality that is possibly a cancer. Presently, biopsy is the only way to confirm the presence of malignancy. There are several types of biopsies, such as fine needle aspiration biopsy, core needle biopsy, and surgical biopsy. Each has its pros and cons. The choice of the type of biopsy to use depends on several factors like, how suspicious the lesion appears, its size, the location in the breast, number of lesions present, other medical problems one may have, and also patients personal preference.

1.5.3.1: Fine needle aspiration (FNA) biopsy

In this, the doctor uses a very thin, hollow needle attached to a syringe to withdraw (aspirate) a small amount of tissue from a suspicious area, which is then observed under a microscope. The needle used for an FNA biopsy is thinner than the ones used for blood tests. On palpating the

abnormal region, the needle can be guided into the area of the abnormality for extracting a biopsy sample. If the lump cannot be recognized on palpation, the doctor might use ultrasound to direct the needle towards and into the mass.

Once the needle is in place, fluid is drawn out. If the fluid is clear, the lump is probably a benign cyst. Bloody or cloudy fluid means it can either be a benign cyst or, very rarely, a cancer. If the lump is solid and small tissue fragments are drawn out, a pathologist will test the biopsy tissue or fluid under a microscope to determine if it is cancerous.

An FNA biopsy has some disadvantages. There is a good probability that this needle can sometimes miss a cancer if not placed among the cancer cells. If cancer cells are found, it is usually not possible to determine if the cancer is invasive. More often, the amount of tissue biopsied may not have enough cells to perform multiple lab tests that are routinely conducted on breast cancer specimens to rule out several possibilities [29].

1.5.3.2 Core needle biopsy

A core biopsy uses a larger needle to sample breast abnormalities palpated by the doctor or diagnosed by ultrasound or mammogram. The needle used in core biopsies is larger than that used in FNA. It removes a small cylindrical core of tissue (about 1/16- to 1/8-inch in diameter and ½-inch long) from a breast abnormality. Several cores are often removed [30]. The biopsy is performed in the presence of local anesthesia. Because it removes larger chunks of tissue, a core needle biopsy is more likely to provide a clear diagnosis than an FNA, although it may still miss some cancers.

1.5.3.3 Vacuum-assisted biopsies

Vacuum-assisted biopsies can be done with systems such as the Mammotome® or ATEC® (Automated Tissue Excision and Collection). For these procedures, a local anesthetic is delivered and a small incision (about ¼ inch) is made. A hollow probe is inserted through the incision into the abnormal area of breast tissue. The probe can be guided into the region of interest by using x-rays or ultrasound (or MRI in the case of the ATEC system). A cylinder of tissue is then suctioned in through a hole in the side the probe, and a rotating knife within the probe cuts the tissue sample from the rest of the breast. Several samples can be taken from the same incision. Vacuum-assisted biopsies are done as an outpatient procedure. No stitches are needed, and there is minimal scarring. This method usually removes more tissue than core biopsies.

1.5.3.4 Surgical biopsy

Most often, it is required to remove all or part of the lesion for microscopic examination. This requires a surgery and hence known as a surgical biopsy or an open biopsy. The surgeon removes the entire mass or abnormal area as well as the surrounding margins of normal-appearing breast tissue. This procedure is called an excisional biopsy. If the mass is too large and only part of it is removed then it is called an incisional biopsy. A surgical biopsy is more involved than an FNA biopsy or a core needle biopsy. It typically requires several stitches and may leave a scar. The larger the amount of tissue removed, the more likely you will notice a change in the shape of your breast afterward. Core needle biopsy is usually enough to make a diagnosis, but sometimes an open biopsy may be needed depending on where the lesion is, or if a core biopsy is not conclusive.

1.5.3.5 Sentinel Node Biopsy and Axillary Node Dissection

Sentinel Node Biopsy and Axillary Node Dissection are performed following a positive biopsy to determine if cancer has spread beyond the breast tissue. The axillary lymph nodes are situated under the arm and the sentinel node is the first axillary lymph node that filters fluid from the breast. Cancer cells found in the lymph nodes suggest that the cancer has metastasized. If the sentinel node is free of cancer cells, then there exists very low possibility of finding malignancy in other nodes [31]. The results of this test are crucial for the patient and the physician in planning the best course of therapy.

1.6 Breast Cancer Treatments:

The treatment strategy varies depending on the grade and stage of the cancer. A localized carcinoma can be removed with local excision (lumpectomy), which is also termed as “breast conserving surgery”. Depending on the extent of breast tissue excision, there are different types of mastectomies. A simple (total) mastectomy removes only the entire breast tissue. A modified radical mastectomy [32] removes the entire breast including the axillary lymph nodes. A radical mastectomy refers to the removal of breast tissue, axillary nodes, and the chest wall muscle under breast. Surgical procedures may be combined with adjuvant therapy such as hormonal therapy, chemotherapy, and/or radiation therapy [33, 34, 35]. In cases of locally advanced breast cancer, “neo-adjuvant chemotherapy” is performed prior to the surgery to reduce the tumor size and eradicate the cancer cells. Radiation therapy uses ionizing radiation (X-rays and gamma rays) to affect cells by activation of radiation-response genes, cell-cycle arrest and radiation-induced cell death. Chemotherapy uses anti-cancer drugs to stop the growth or multiplication of cancer cells. Since these drugs work most effectively on cells that divide rapidly, it kills cancer cells more effectively than normal cells.

CHAPTER 2

THEORY

The work presented in this thesis makes use of a number of theoretical principles. The main techniques used throughout this study are time-resolved fluorescence lifetime spectroscopy and reflectance spectroscopy. The fundamental optical theory behind these two techniques is presented in this chapter.

2.1 Fluorescence Lifetime

Molecules have discrete energy levels, which depend on the rotational, vibrational and electronic structure of the specific molecule. The ability of a molecule to absorb and emit radiation is dependent on these characteristic energy levels. When a molecule absorbs a photon of light whose frequency corresponds to the difference between the energy levels, it can promote transition of the electrons from the ground state to an excited state. Depending on the structure of the molecule, the frequencies absorbed by that molecule are determined. Light absorbed by a molecule is predominantly converted to heat; however an absorbed photon can be re-emitted as Fluorescence.

Any molecule in an excited state has the affinity to return to the ground state, during which emitting the absorbed energy *via* number of processes. The two broad classification of de-excitation are non-radiative and radiative decay processes. A Jablonski diagram illustrates these processes and the energy levels for a typical photo-luminescent molecule. A molecule initially occupies the lowest vibrational energy level, called the Singlet state and labeled $S_{o.}$

On absorbing a photon of the correct energy, it can be excited to one of several vibrational energy levels in the first excited state, S_1, or to higher electronically excited singlet states (e.g. S_2). Relaxation to the ground state can either be emission less or involves emission of a photon. In Fig below, the straight vertical arrows represent fluorescence and phosphorescence, which involve the release of a photon of energy. If deactivation by fluorescence is rapid compared to radiation less processes, then the fluorescence intensity is higher.

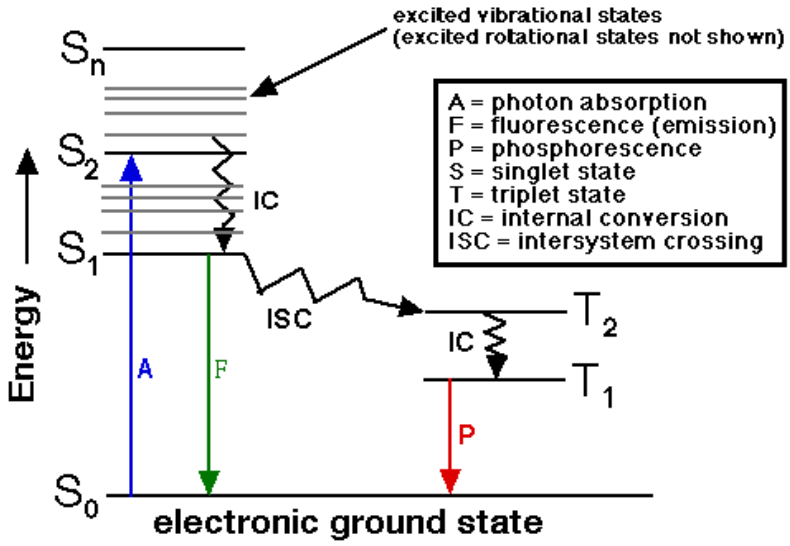

Fig 2.1: A Jablonski diagram or partial energy level diagram for a photo-luminescent system showing pathways for the deactivation of an excited state. [59]

On de-excitation, fluorescence may return the excited molecule to any of the vibrational energy levels in the ground electronic state. Hence fluorescence can be observed over a range of wavelengths. The change in energy for the fluorescence transition is generally less than that for absorption, the resulting fluorescence spectrum being shifted to a longer wavelength than its absorption spectrum (Fig 2.2). This is a consequence of the efficiency of vibrational relaxation to the lowest vibrational level in an excited state, and is called the Stokes shift. The Stokes shift is

defined as the difference between the maximum of the first absorption band and the maximum of the fluorescence spectrum (Fig 2.2).

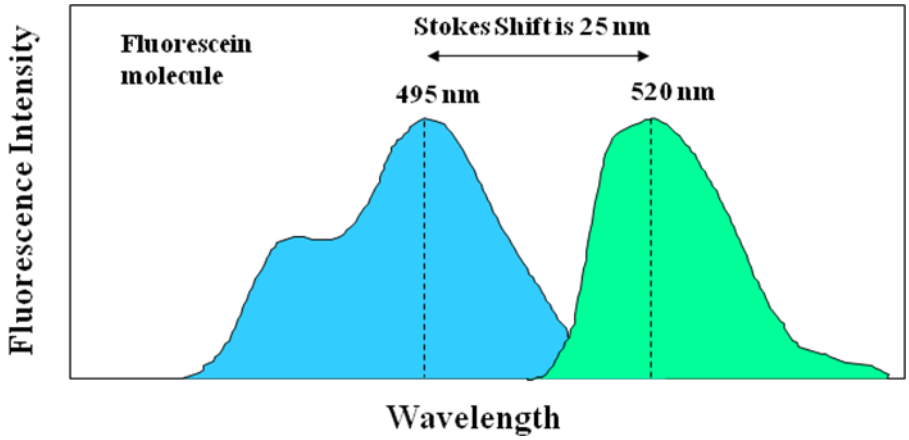

Fig 2.2: Diagram illustrating the Stokes shift observed between the excitation (blue) and emission (green) spectra. [60]

2.1.1 Fluorescence Decay Kinetics

A population of excited fluorophores [M] decays in accordance with the first order kinetic process.

$$-\frac{d[M]}{dt} = k_F[M] \quad \text{..... Eq.1}$$

Where the rate constant, k_F, is the sum of the rate constants for all the radiative and non radiative decay processes ($k_F = k_R + \sum k_{NR}$) [36]. Therefore kF = k_R + k_{IC} (Internal conversion) + k_{ISC} (Intersystem crossing) + k_{VR} (Vibrational and Rotational) + $k_{quenching}$ +….. .

Following integration of Equation 2.1, the concentration of the excited state as a function of time is obtained to be

$$[M](t) = [M]_0 \exp(-k_F t) \quad \text{..... Eq.2}$$

Where $[M]_o$ is the initial concentration of M at t=0. The parameter monitored during fluorescence lifetime experiments is the fluorescence intensity, I, which is the rate of the emission of photons and is related to the excited state concentration by

$$I_F(t) = k_R[M](t) \quad \text{..... Eq.3}$$

Substituting for [M] from Equation 2.2 gives

$$I_F(t) = k_R[M]_0 \exp(-k_F t) \quad \text{..... Eq.4}$$

Substituting for $[M]_o$ from $I_F(0) = k_R [M]_0$, where $I_F(0)$ is the intensity at the time of the initial excitation pulse, into Equation 2.4 gives

$$I_F(t) = I_F(0)\exp(-k_F t) \quad \text{.....Eq.5}$$

Therefore the intensity decays exponentially after the initial excitation pulse. The fluorescence lifetime of the excited state, τ_F, can be represented as $\tau_F = (1/k_F)$. The fluorescence lifetime of a molecule is defined as the time taken for the excited state population to fall to 1/e of its intensity of that initially excited.

Equation 2.5 can then be rewritten as

$$I_F(t) = I_F(0)e^{\frac{-t}{\tau_f}} \quad \text{.....Eq.6}$$

Equation 2.6 relates the measured parameter of intensity to the fluorescence lifetime and enables its calculation experimentally.

2.1.2 Fluorescence Quantum Yield

The efficiency of fluorescence can be expressed by the fluorescence quantum yield, ΦF, which is the fraction of excited molecules returning to the ground state by fluorescence (Equation 2.7).

$$\Phi = \frac{Number\ of\ photons\ emitted}{Number\ of\ photons\ absorbed}$$

The quantum yield ranges from 1, wherein every molecule in an excited state undergoes fluorescence, to 0 where fluorescence does not occur. The fluorescence quantum yield, ΦF, can be related to the fluorescence lifetime by

$$\Phi = \frac{k_R}{k_F} = k_R\tau_F$$

Therefore the fluorescence lifetime, τ_F, is a measure of the fluorescence quantum yield, ΦF. The rate constant for the radiative decay processes, k_R, is essentially constant for a particular fluorophore as it is a consequence of the intrinsic electronic properties of the molecule. Therefore the fluorescence lifetime is sensitive to changes in the non-radiative decay pathways. A subsequent increase in non-radiative decay rates will reduce the fluorescence lifetime. These effects make the fluorescence lifetime extremely sensitive to the molecular environment surrounding the fluorophore.

2.1.3 Advantages of lifetime measurements

The intensity of the fluorescence is proportional to the amount of the radiation from the excitation source that is absorbed and the quantum yield for fluorescence. The intensity of fluorescence increases with an increase in quantum efficiency, incident power of the excitation source and concentration of the fluorescing species. Fluorescence lifetime is an intrinsic property of the fluorophores and is independent of the concentration of the fluorescing species and the incident power of the excitation source. Therefore, the fluorescence lifetime is insensitive to fluctuations or variations in the excitation source, optical loss in optical path, optical aberrations, and fluorophore concentration and photo-bleaching.

2.1.4 Auto-fluorescence of breast

The most important auto-fluorophores that are endogenous to cells and tissues are the amino acids, the essential building blocks of proteins and enzymes, NADH and FAD, which regulate cell metabolism, porphyrins, structural proteins responsible for rigidity and flexibility of tissues and organs, and fluorescent pigments like melanin etc [37,38].

During progression of a disease, like Breast Cancer, the local environment in which fluorophores are embedded changes, as well as their relative concentrations. In our study, we observe the fluorescence lifetimes of Flavins, Lipopigments and Porphyrins. Due to the presence of multiple fluorophores with distinct lifetimes, the overall decay function for any given pixel will be inherently multi-exponential with each component reflecting a fractional contribution of an individual fluorophore.

2.2 Reflectance

2.2.1 Basics of Reflectance

All materials have a complex index of refraction: $m = n - jK$ …… Eq 1.

Where, m = Complex index of refraction, n = Real part of the index and j = (-1)1/2

K = Imaginary part of the index of refraction, sometimes called extinction coefficient.

When photons enter an absorbing medium, they are absorbed according to the Beer-Lambert Law. The absorption coefficient is related to the complex index of refraction by the following:

$\varepsilon = 4K/\lambda$ ……Eq.2

The reflection of light, R, normally incident onto a plane surface is described by the Fresnel equation:

$R = [(n - 1)2 + K2] / [(n + 1)2 + K2]$ ……..Eq.3

At angles other than normal, the reflectance is a complex trigonometric function involving the polarization direction of the incident beam.

Consider the simple Beers-Lambert Law:

$A = - \log_{10} (I_T/I_o) = -\varepsilon dc$

Where: I_T is the monochromatic radiant power transmitted by the absorbing medium, I_o is the monochromatic radiant power incident on the medium, T_i is the internal transmittance (=IT/Io), ‘ε’ is the molar absorption coefficient, ‘c’ is the amount concentration, ‘d’ is the absorption path length, ‘A’ is the absorbance. In transmission, when light passes through a slab of material, there is little or no scattering. In reflectance, however, the optical path of photons can be visualized as a random walk. At each grain of the slab material, a certain percentage of photon, on striking, are absorbed [39, 40].

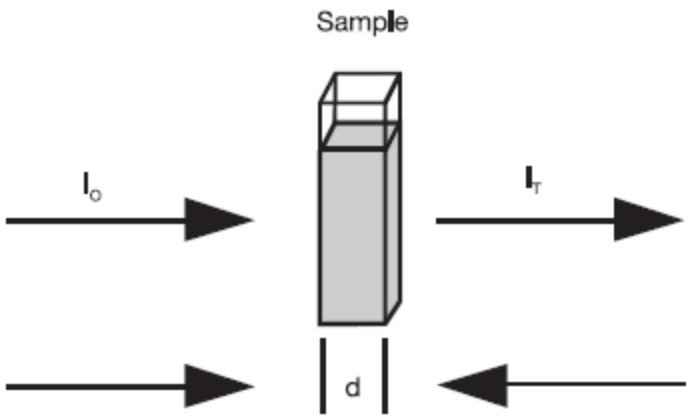

Fig 2.3: Beer–Lambert's absorption and transmission of a beam of light as it travels through a slab of material with thicknesses d. [61]

If the grains that make up the slab are dark, the majority of photons will be absorbed at each encounter and essentially all photons will be absorbed in only a few encounters. This process also enhances weak features not normally seen in transmittance, further increasing reflectance spectroscopy as a diagnostic tool. In a mixture of light and dark grains (e.g. quartz and magnetite) the photons have such a high probability of encountering a dark grain that a few percent of dark grains can drastically reduce the reflectance, much more than their weight fraction. A general rule with mixtures is that at any given wavelength, the darker component will tend to dominate the reflectance. The amount of light scattered and absorbed by a grain is dependent on grain size. A larger grain has a larger internal path where photons may be absorbed according to the Beers-Lambert Law. It is the reflection from the surfaces and internal imperfections that influence the scattering. In a smaller grain there are proportionately more surface reflections compared to internal photon path length, or in other words, the surface-to-volume ratio is a function of grain size [40].

Reflectance Spectroscopy is the based on application of above mentioned phenomenon to study light that has been reflected or scattered from a surface. As photons enter into a tissue, some are reflected from the tissue surface, some pass through the same, and some are absorbed. Those photons that are reflected from the tissue surface or refracted through a tissue particle are said to be scattered. Scattered photons may encounter another scatterer or be scattered away from the surface so they may be detected and measured [41].

Reflectance spectroscopy is increasingly being used to for tissue characterization and classification. Diffusion approximation has been widely researched to study the light propagation in the Biological tissues. It is necessary to develop computational techniques to enumerate the physiologically correlative components of the tissues for detection and differentiation of biological samples.

2.2.2 Reflectance of Breast

The measured reflectance spectrum contains both diffuse reflectance as well as singly backscattered light [42]. The absorption spectrum of tissue depends on type of predominant absorbing molecules or chromophores and therefore provides information about its chemical composition. Water is a strong absorber in both UV and IR regions. DNA and proteins absorb in the UV region, while hemoglobin, melanin and β-carotene in the visible range.

Since cancer cells and normal cells have different morphologies, their optical properties also differ. Changes in architectural and morphological features as a result of cancer progression, including increased nuclear/cytoplasmic ratio, hyperchromasia, and pleomorphism, affect the nature of the scattering events when light interacts with the tissue.

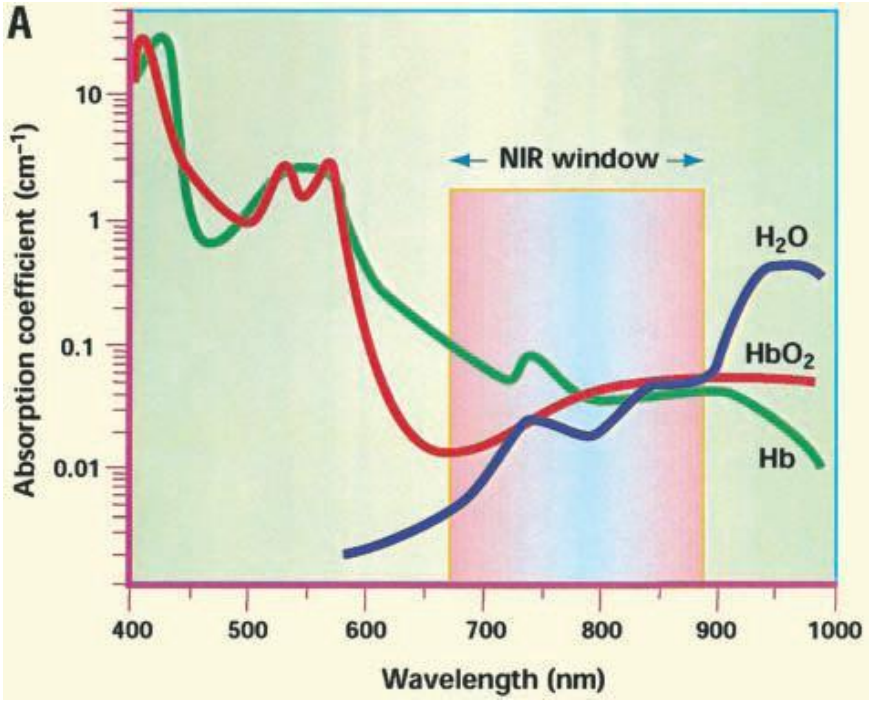

Fig 2.4: Absorption spectra of biological tissue [62]

Therefore, these changes complicate the interpretation of spectra as they relate to tissue disease status. For example, cancer cells are well documented to have increased nuclear size, and decreased cell differentiation due to the abnormal duplication of cancerous cells. Larger nuclei result in more backward scattering events, which leads to the collection of more light at the optical fiber. Therefore, the light intensities can be used, to some extent, as features for diagnostic decisions. The spectral distribution may also be altered by the concentration of hemoglobin [43, 44]. Initially, non-necrotic cancerous tissues contain a higher concentration of hemoglobin due to the increased consumption of more nutrients than normal cells. Clearly, tissues containing different oxy- and deoxy-hemoglobin concentrations will have different spectra [45].

CHAPTER 3

EXPERIMENTS

The two main diagnostic techniques employed within this thesis to investigate diagnosis of cancer were Time Correlated Single Photon Counting (TCSPC) and Optical reflectance spectroscope. A generic description of these techniques and the relevant theory is presented within this chapter. Furthermore, sample preparation and experiment implementation are also discussed.

3.1 Sample Preparation

Ten sets of breast tissue samples were obtained from patients undergoing breast cancer surgery (lumpectomy or mastectomy) at the University of Texas Southwestern Medical Center, Dallas. Auto-fluorescence and reflectance spectra were measured from freshly excised breast tissue samples immediately after excision. Optical measurements were made at a cancerous site, an adipose site and a remote normal tissue site.

After each surgery, in case of both mastectomy and lumpectomy, the surgeon removed the specimen and then placed surgical clips and sutures to orient the specimen for pathological assessment. The pathologist weighed the specimen and performed inking to define orientations and to identify tumor proximity to specific margins. The specimen was sliced into multiple sections and palpated for masses or lesions. In order to obtain optical measurements on the excised breast samples, it was made sure that the carcinomas found after grossing were a clearly identifiable mass lesion.

Auto-fluorescence Spectroscopy and Reflectance spectral imaging was performed on the regions specified as Fibrous, Cancer and Adipose tissues of the lumpectomy/mastectomy specimens between 10 and 20 minutes after excision. The surgeons also performed sentinel lymph node dissection in addition to the partial mastectomy on a subset of patients. For sentinel lymph node dissection, Technetium Sulfur Colloid and Isosulfan Blue, in combination were used to trace the lymphatic drainage of a neoplasm to its Sentinel lymph node. In these cases, the Isosulfan Blue was found within the lumpectomy margins in varying degrees. Sites were considered to have too much Isosulfan Blue, if the intensity of the reflectance spectrum at 650 nm was lower than the intensity at 450 nm, indicating that Isosulfan Blue has overwhelmed by the hemoglobin absorption. Such recordings were excluded from further analysis.

Histological diagnoses were further obtained for each tissue specimen from microscopic evaluation of Hematoxylin and eosin (H&E) sections within a depth of 2 mm from the probe-tissue contact surface (marked by an ink spot). When malignancy presented anywhere within the depth of histological evaluation, the sample diagnosis was designated as being malignant. If a benign or normal sample exhibited heterogeneous tissue composition, the sample histology was designated to be the predominant tissue type immediately below the tissue surface where the optic probe was placed.

3.2 Time Correlated Single Photon Counting Unit (TCSPC)

Time correlated single photon counting (TCSPC) is an experimental technique employed to perform the time-resolved fluorescence spectroscopy used within this study to measure the fluorescence lifetimes of intrinsic fluorophores present in the Breast tissue sample.

3.2.1 The principle of TCSPC

On excitation with a short pulse of light, the intrinsic tissue fluorophores absorb the energy emitting fluorescence. This first photon fluorescing is detected and the time interval between the excitation and detection of the photon is recorded [46]. This procedure is continuously repeated for a complete distribution of individual photon arrival times at the detector. The fluorescence lifetime(s) of the fluorophores sample is then calculated from this recorded fluorescence intensity decay plot. Fig 4.1 displays a generic experimental setup typically used for TCSPC techniques.

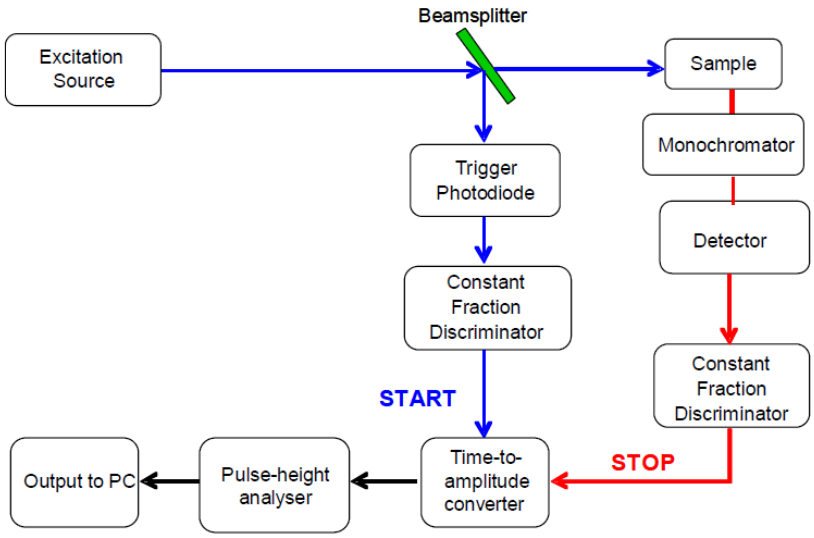

Fig 3.1: A generic setup necessary to perform TCSPC measurement [63]

Every excitation pulse triggers an electronic 'START' pulse for the timing, since a fraction (~10%) of the excitation pulse is being directed towards a fast photodiode, using a beam splitter, to convert the optical signal to a triggering pulse (the 'START' pulse). The electrical pulse then passes through a constant fraction discriminator to minimize variations in the trigger timings and to a device analogous to a stopwatch called the time-to-amplitude converter.

The time-to-amplitude converter can be considered as a capacitor which begins charging when triggered by the 'START' pulse and stops when triggered again by a 'STOP' signal. The threshold differentiation for the START pulse was set at -300 mV; therefore, START pulses with a magnitude below the threshold did not trigger the time-to-amplitude converter. The amplitude of the pulse could be varied depending on the incident light intensity on the photodiode [47].

The remainder of the excitation pulse that is reflected off the beam splitter is directed towards the sample and the emission of photons by fluorescence is detected. The TCSPC detector operates by converting the emitted photon energy into an electrical pulse. The 'STOP' pulse, produced by the first detected photon, passes through a constant fraction discriminator and then halts the voltage ramp at the time-to-amplitude converter. Then, the time-to-amplitude converter is discharged to allow the electrical signal to be quantified, as this is proportional to the time between the start and stop triggers. A pulse-height analyzer converts the electrical signal into a digital signal. This is recorded as a single count on a histogram of fluorescence intensity against time. Typically hundreds of thousands of these counts are registered to display an exponential decay curve, which allows the calculation of the fluorescence lifetime of the fluorophores.

3.2.2 TCSPC Components

Micro-channel plate

A micro-channel plate (MCP) photo-multiplier tube was used to detect single photons and convert their energy into electrical signals [47]. The MCP is a metal plate, containing channels with an internal diameter of between 6 μm and 25 μm, which is sandwiched between a photo-anode and cathode. The function of the channels is to amplify an initial electronic signal following the impact of an arriving photon on the photocathode (Fig 4.2).

The collision of the photon causes the emission of a photoelectron from the cathode, which is accelerated towards the anode by a potential difference across the MCP. During transit the photoelectron collides with the channel walls, which are lined with dynode material. The impact causes the emission of secondary electrons and subsequent repetition of this process leads to a logarithmic increase in the current of the channel. The initial current can typically be amplified 10000 times using this method to provide a measurable current at the anode.

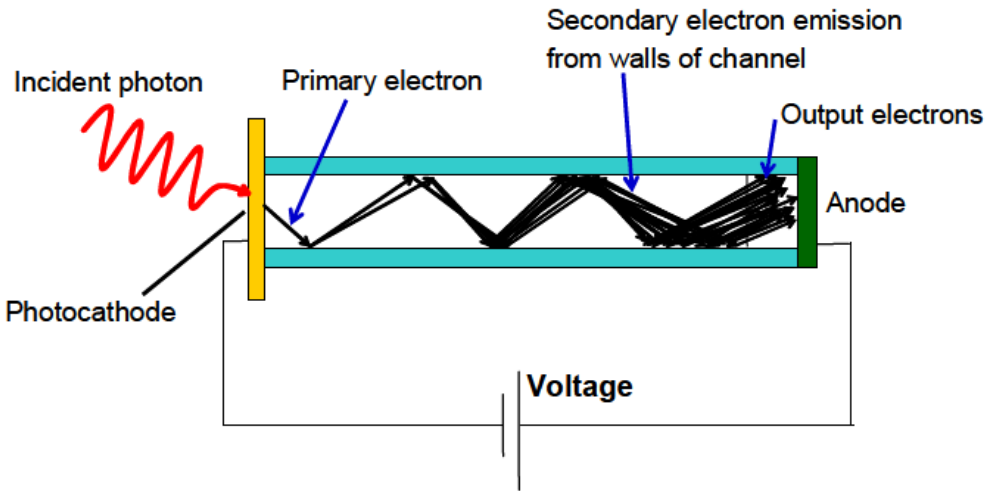

Fig 3.2: The operating mechanism of an isolated channel from a micro-channel plate photomultiplier tube. [63]

In TCSPC, the time resolution of the system is heavily dependent on the variation in the time taken for electrons to pass through the detector. This transit time spread (TTS) increases the uncertainty in the photon arrival timing and occurs due to the numerous possible routes through the PMT channels providing a distribution of photon arrival times. Fig 3.2 pictorially illustrates this phenomenon, where the single incident photon produces a multitude of output electrons with different transit times. The micro-channel plate employed for TCSPC has a transit time spread of 25ps.

Time-to-amplitude converter (TAC)

The time-to-amplitude converter (TAC) produces an electrical pulse whose amplitude is proportional to the time interval between the start and stop pulses. The start pulse triggers the TAC to begin accumulating charge, which continues until a stop signal is detected. The capacitor is then discharged and the amplitude of the electrical output pulse is related to the time lapsed. The TAC is then reset to commence a new cycle. During the discharge and resetting period no incoming signals can be detected. This is referred to as the 'dead time' of the TAC and is less than 150 ns in duration for the system used to record decays curves throughout this study.

If the count rate (rate at which photons are recorded) is too high, this can result in more than one pulse arriving at the TAC during a single cycle. This phenomenon called pulse pile-up can introduce errors into the timings of the photons as the first photon will be recorded. This results in a bias of the TAC to record shorter lifetimes. This problem can be avoided by ensuring that the count rate is considerably lower than one photon per excitation pulse. This makes sure that the probability of a second photon arriving in the same excitation cycle is extremely low. Therefore, a true representation of the exponential decay curve is recorded.

Constant Fraction Discrimination

The electronic pulse output signals from the photodiode (START trigger signal) and the photo-multiplier tube detector can vary in amplitude, which can affect the timing of the trigger signals detected by the time-to-amplitude converter. This effect is illustrated in Fig 4.3, which shows the time variation in detecting a pulse based on a threshold voltage level, for pulses of different amplitudes. This form of pulse detection (leading edge discrimination) is dependent on the leading edge of the pulse reaching a threshold value to trigger the timing.

Using leading edge discrimination results in the spread of timings hence increasing the timing uncertainty and broadens the instrument response function.

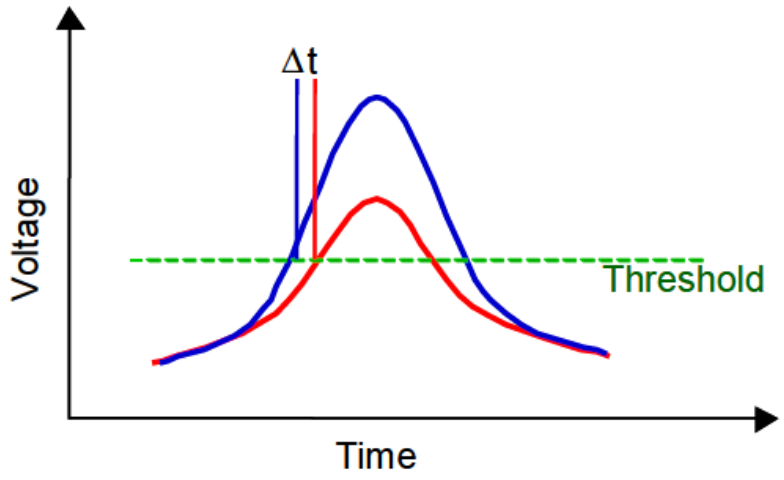

Fig 3.3**:** Illustration of timing variation from employing leading edge discrimination techniques to detect pulses. [63]

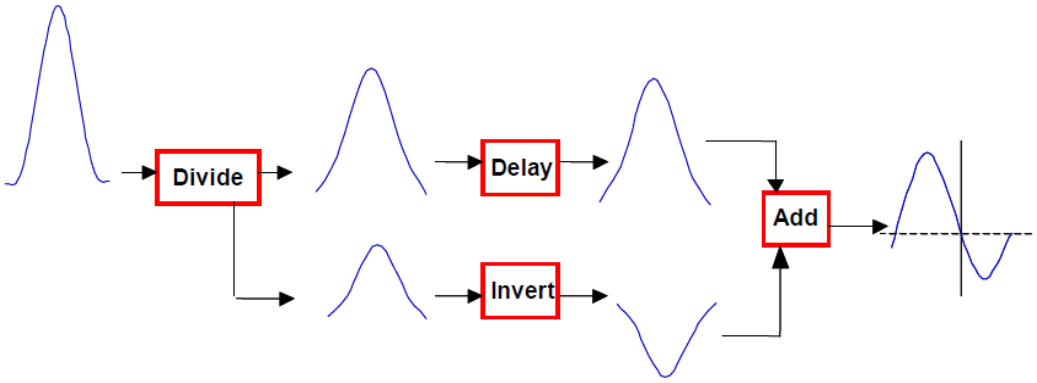

Fig 3.4: Schematic illustrating the technique of constant fraction discrimination [63].

To overcome this timing uncertainty, the technique of constant fraction discrimination is employed.

This technique, as illustrated in Fig 3.3, divides the incoming pulse, by a pre-determined fraction usually 2/3 or 1/3, to create two pulses. The smaller fraction pulse is inverted, whilst the other is delayed by half the pulse width. The two pulses are then recombined to provide a profile with a potential that crosses zero at a point that is independent of the amplitude. This ensures the consistent timing of pulses for time-resolved experiments.

3.3 Optical Reflectance Spectrometer

3.3.1 The principle of Spectrometer

Light enters the optical fiber to be transmitted into the spectrometer. Once in the spectrometer, the divergent light emerging from the optical fiber is collimated by a spherical mirror. The collimated light is diffracted by a plane grating, and the resulting diffracted light is focused by a second spherical mirror. An image of the spectrum is projected onto a linear CCD array, and the data is transferred to a computer through an onboard A/D converter [48, 49].

Light strikes onto the photodiodes with CCD pixels. These reverse-biased photodiodes discharge a capacitor at a rate proportional to the photon flux. When the integration period of the detector is complete, a series of switches closes and transfers the charge to a shift register. After the transfer to the shift register is complete, the switches open and the capacitors attached to the photodiodes are recharged and a new integration period begins. At the same time that light energy is being integrated, the data is read out of the shift register by an A/D converter. The digitized data is then displayed on your computer.

3.3.2 Spectrometer Components

In fig 3.5, Label 1 depicts the SMA 905 through which the light enters the optical bench. The amount of light and wavelength which enters the spectrometer is regulated by the Slit (2) and

the Filter (3). SAG+, Ag-coated collimating mirror (4) focuses the selected wavelength regions onto the grating (5). The light is received by the focusing mirror (6) which in turn reflects the light onto the L2 Detector Lens (7).

The Detector (8) then converts the optical light into a digital signal. Every pixel on the CCD array detector responds to the respective wavelength of light that strikes it and transmits the response to the software application.

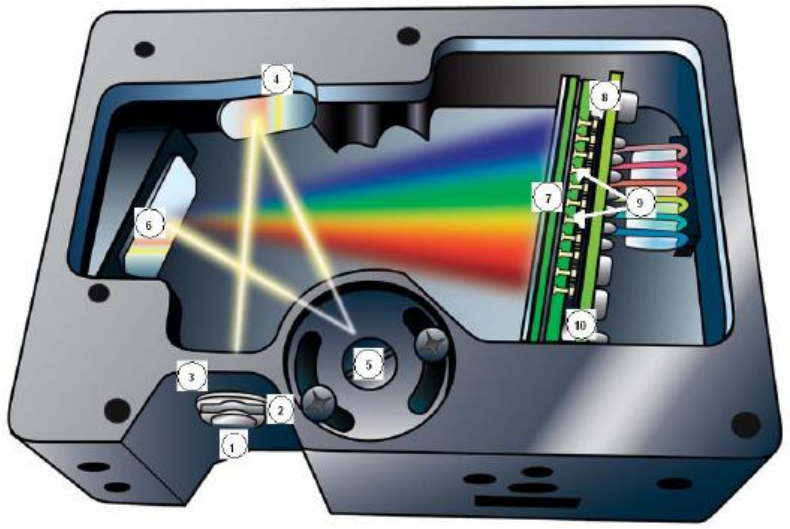

Fig 3.5: The internal working mechanism of the USB 2000 spectrometer. [64]

3.4 Implementation

For Auto-Florescence Lifetime Measurements a custom made single channel TCSPC (ISS Inc., Champaign, IL) machine is employed. This system consists of a 12 V power supply unit, a

stepper motor which is driven by a 5 slot filter wheel used in excitation wavelength selection. In addition an emission filter, a continuous variable Neutral Density (ND) filter for excitation light intensity control and a highly sensitive cooled PMT (Becker & Hickl GmbH) with wavelength sensitivity ranging between 125 – 850 nm is also employed. Instrument automation was achieved through an ISS-PCMC card and a motion control box. The PMT gain was controlled via PC based card (DCC-100).

A picosecond (ps) broadband (400 – 1800 nm) pulsed laser (SC - 450, Fianium Inc., Eugene, Oregon) is used as an excitation source at the repetition rate of 20 MHz A PC based single photon counting card (SPC- 130) is used in achieving precise synchronization between incoming laser pulse and the photon event. The laser is coupled to the source fiber of the bifurcated optical probe (core diameter 100 μm) and resulting fluorescence emission was collected through the detector fiber (400 μm core diameter).

LRS system consists of a tungsten-halogen light source (HL2000HP, Ocean Optics, Dunedin, FL, USA), a CCD array spectrometer (USB 2000+, Ocean Optics, Dunedin, FL USA), and a laptop computer. The spectrometer had a spectral range ranging from 460nm-1150nm. A custom made bi-furcated fiber optic probe (Fiber guide Industries, Stirling, NJ, USA), with 100μm source and detector diameters, and 100μm separation was used for the measurements. The probe was fixed on a stereotactic frame in order to control the position, and minimize the pressure on the tissue surface.

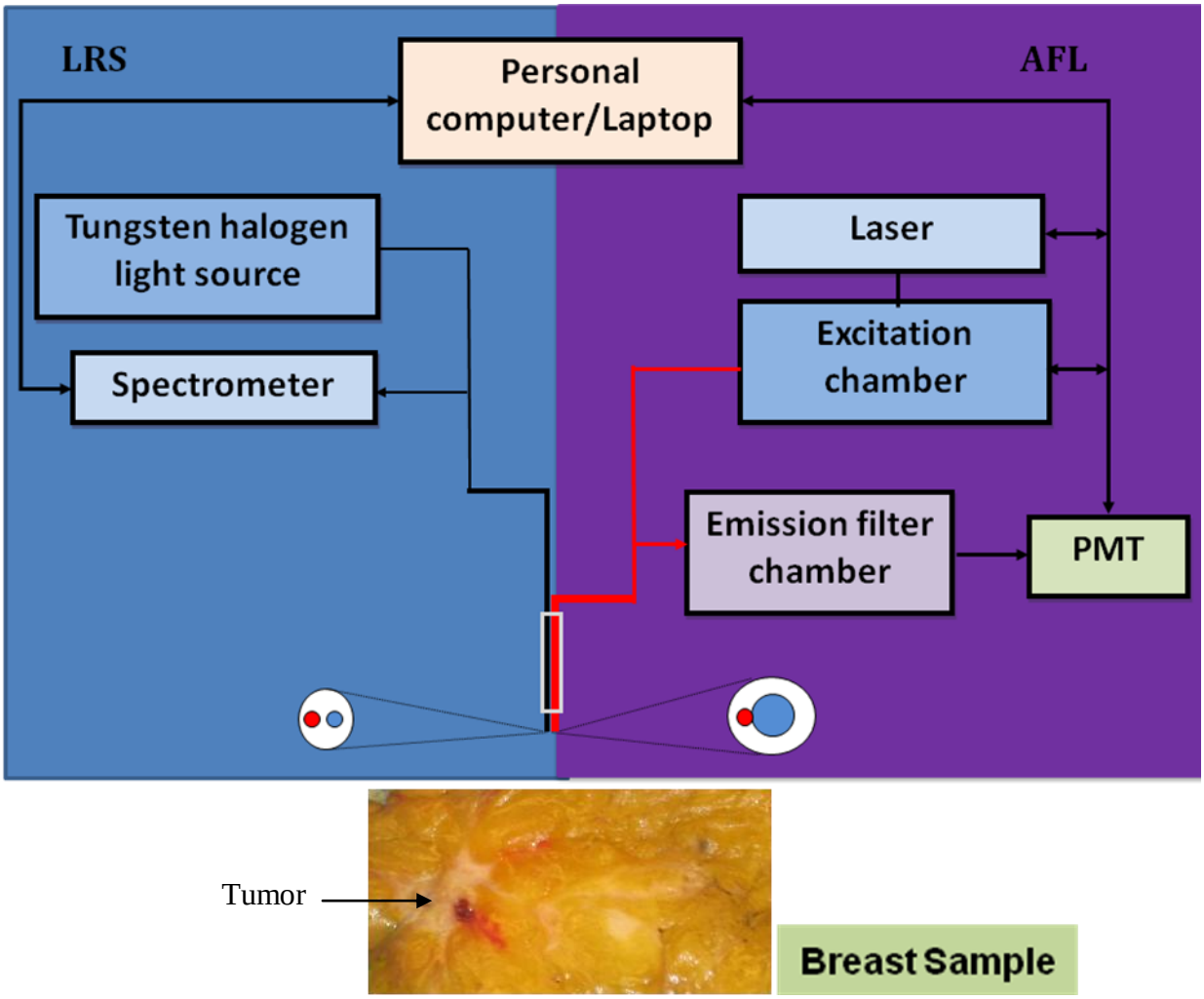

Fig 3.6: A block diagram illustrating experimental set-up for LRS system (left) and AFLM system (right). A closer view of bi-furcated fiber tips are shown for each fiber (red = source; blue = detector).

Multiple data points were than obtained by placing the probe at different spatial location on the tumor tissue and then the normal tissue. On an average, 5 data points were obtained for each tissue type.

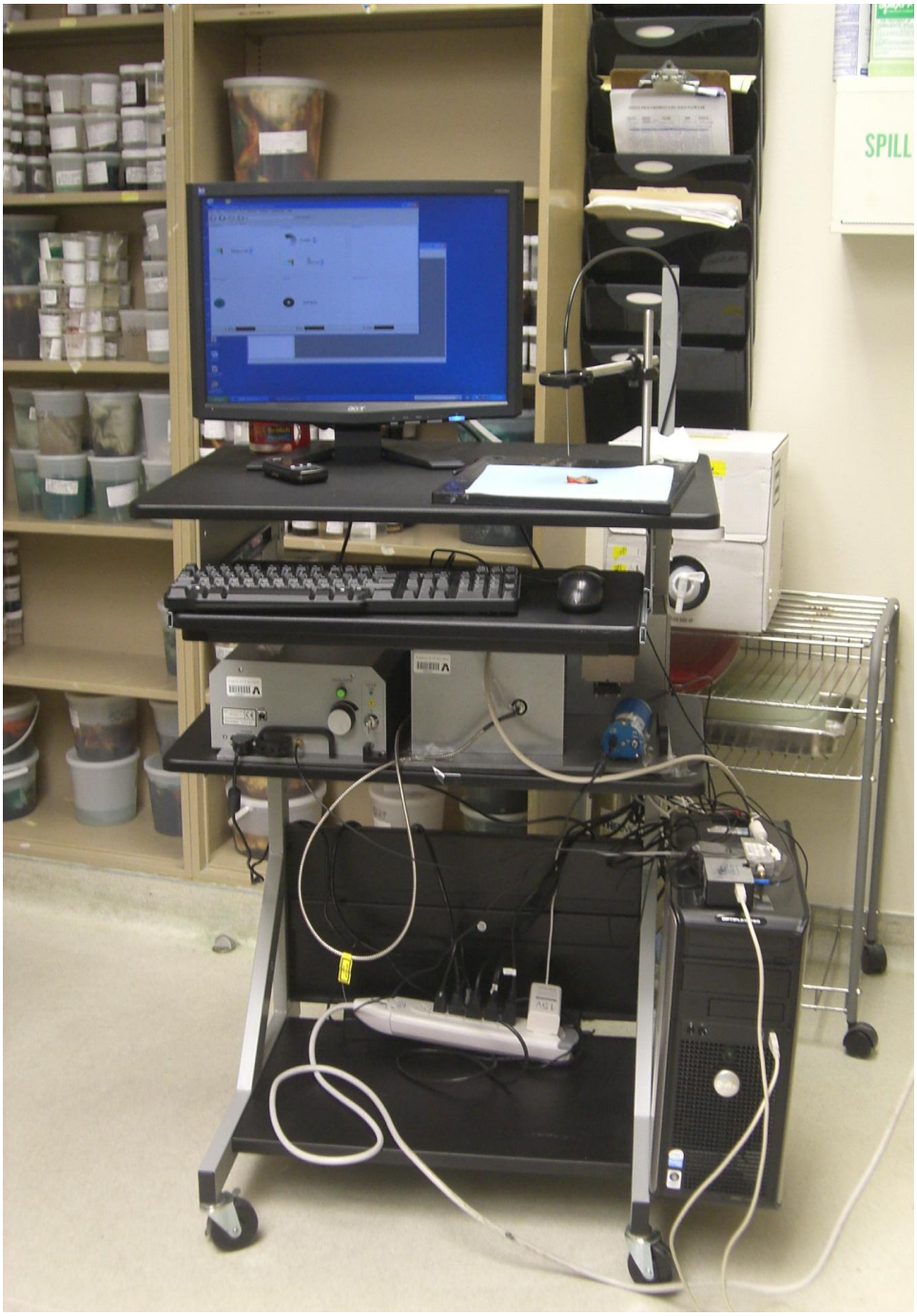

Fig 3.7: Experimental set up used in acquisition of data from ex vivo breast samples.

CHAPTER 4

RESULTS AND DISCUSSION

Preliminary results indicate that the auto-fluorescence lifetime and reflectance together, may not only contain diagnostic information, but also is accurate in differentiating normal ductal epithelium from invasive ductal carcinoma. Readings were acquired from the breast specimens after the patients had undergone complete or partial mastectomy. The data was acquired at the University of Texas Southwestern Medical Center, Dallas under the guidance of Dr. David Euhus. Dr. Euhus is a renowned surgeon for carrying out mastectomy and lumpectomy surgeries on breast.

4.1 Experimental Protocol

The specimens extracted during surgery, were kept frozen and delivered to the pathology room. First, the tumor size was measured and noted. The pathologist then grossed the sample and palpated the specimen, to feel lumps or masses, in order to determine the malignant region. The data for auto-fluorescence lifetime and reflectance were acquired on the same locations from both normal and malignant regions of the breast.

The background light was initially recorded with the room lights and the light source switched off. A reference lifetime and reflectance spectra were collected in case of every breast sample prior to data acquisition. The probe was placed on the locations identified by the pathologist, as normal fibrous, adipose and cancerous tissue. After lifetime spectra were obtained for all the four wavelengths, the TCSPC unit was switched off. The spectrometer was then switched on to record the reflectance spectra from the same location

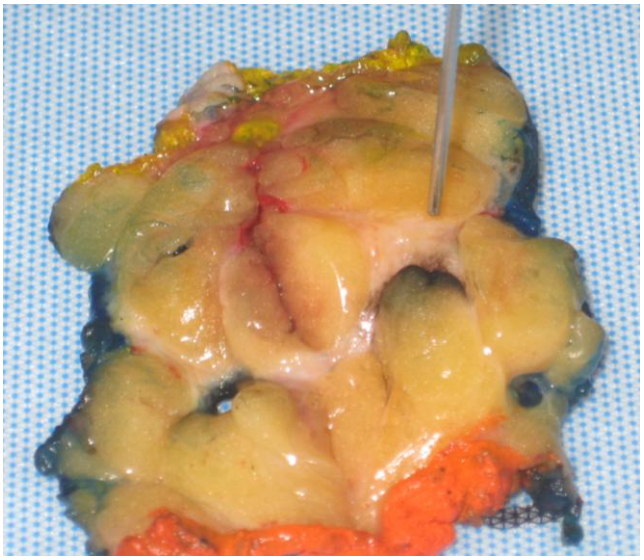

Fig 4.1: Illustrates a probe used for acquiring data from the breast sample.

Following data acquisition, specimens were marked with India ink to indicate the region sampled. The tissue were then cut through the marked locations and put into separate cassette holders, labeled as “Optical study”, and fixed in formalin.

The data that were used for analysis of lifetime and reflectance spectra were from seven patients who had biopsy-proven invasive ductal carcinoma of the breast, and no prior history of pre-surgical chemotherapy. Auto-fluorescence and reflectance spectroscopy measurements were priorly obtained out of ten patients out of whom three cases had to be discarded due to their prior exposure to radiation with pre-surgical chemotherapy and presence of excess Isosulphan blue used during surgery. A total of 37 cancer and 36 normal auto-fluorescence lifetime spectra were retained for further statistical analysis. Similarly, 34 cancerous and 31 normal reflectance curves were investigated with further analysis to determine significance in diagnosing cancer from normal ductal epithelium.

4.2. Data Analysis

AFLM data analysis

Flavins, Lipopigments and Porphyrins are the endogenous fluorophores targeted to obtain auto-fluorescence, as a contrast parameter to differentiate cancer from healthy tissue. In order to achieve optimum excitation of all three endogenous compounds, an excitation wavelength of 447 nm was chosen. While keeping the excitation wavelength constant, the emission wavelengths were changed between 532 nm, 562 nm, 632 nm and 684 nm. Filter selection and data collection were done through ISS Inc. provided Vinci software. The optical probe was placed at a distance of ~1 mm away from the surface of the tissue and in-vivo fluorescence data were collected from 6 random positions from the exposed tumor and healthy tissue for each emission wavelength [50]. The detected fluorescence decay at each tissue position was imported into Matlab (The Mathworks Inc., Natick, MA) and normalized with respect to the peak intensity. In order to quantitatively differentiate auto-fluorescence decay of cancer and control, each curve was fitted (least square non-linear fitting algorithm) by a two component exponential model, given as:

$$Intensity(I) = \sum_i a_i e^{\frac{-t}{\tau_i}}$$

where, $\tau_{i\ (i=1,\ 2)}$ indicates lifetime of each component and $A_{i\ (i=1,\ 2)}$ is intensity contribution of each component on the overall fluorescence decay. The mean lifetime was calculated using the following equation:

$$< \tau > = \frac{\sum_i a_i \times \tau_i^2}{\sum_i a_i \times \tau_i}$$

LRS Data Analysis

Each acquired spectrum was divided by the reflectance spectrum obtained from a diffuse reflectance standard (WS-1, Ocean Optics, and Dunedin, FL, USA) to eliminate the effect of the light source, fibers and detector from the reflectance spectrum [51]. Only the spectrum ranging from 500nm-850nm was selected for further analysis. Spectral slope, using linear regression, was calculated over particular windows in the spectrum that had physiological significance. The four windows that showed significant difference ($p < 0.05$) were selected for further statistical comparisons. With the use of a generalized linear regression mixed model, we compared the predictive power of the reflectance technique. Further, by generating the Receiver Operating Characteristics (ROC) curve the sensitivity and specificity that can be achieved was determined.

Generalized Linear Regression Mixed Models (GLMM)

GLMM provides a flexible way to model data sets that do not satisfy the assumptions of a linear mixed model. An extension of generalized linear model (GLM) is the GLMM which incorporates normally distributed random effects apart from the fixed effects [52]. A GLMM can be defined in terms of several model components:

- A linear predictor η that is a linear combination of regression coefficients: $\eta = X\beta + Z u$ is used to model the relationship between the fixed and random effects. The residual variability contained in the residual, e, of the linear mixed model equation is incorporated in the variance function of the generalized linear mixed model.
- An inverse link function $\mu_i = h(\eta_i)$ is used to model the relationship between the linear predictor and the conditional mean of the observed trait.
- A variance function, $v(\mu_i, \Phi)$ is used to model the residual variability.

The linear mixed model assumes that the relationship between the mean of the dependent variable y and the fixed and random effects can be modeled as a linear function, that the variance is not a function of the mean, and that the random effects follow a normal distribution.

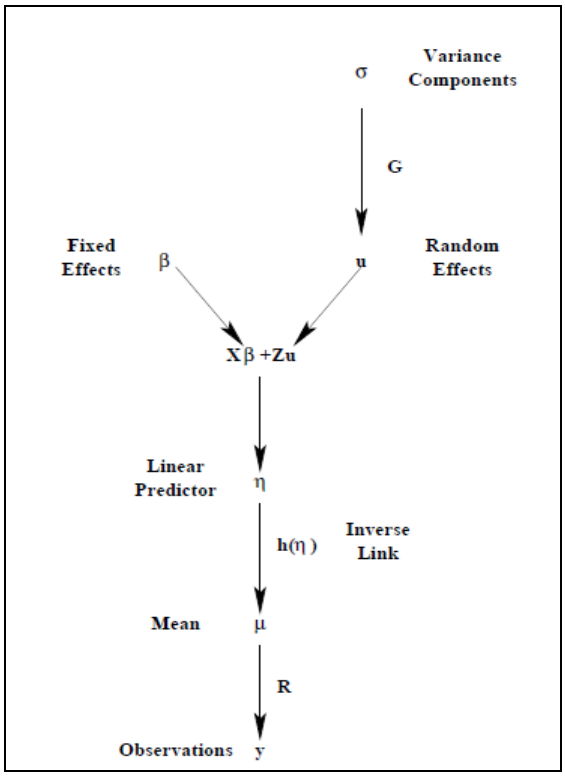

Fig 4.2: A symbolic representation of Generalized Linear Regression Mixed model [65].

A two-sample unequal variance test was used (on the means) to determine whether statistically significant differences between tissue types in parameters extracted from the auto-fluorescence lifetime and diffuse reflectance spectra. GLMM was applied for estimating Receiver Operating Characteristic curve using repeated measures on reflectance parameters that were identified with a p-value less than the confidence limit of 0.05.

4.3 Results and Discussion

The mean lifetime was calculated for each emission wavelength and averaged over 7 breast cancer cases. Fig 4.3 shows the comparison for averaged mean lifetime between cancer and normal breast tissue. It can be noticed from the plot below that the averaged mean lifetime for normal is greater than that of malignant tissue in two wavelengths, 532 nm and 562 nm. However, in case of 632 nm and 684 nm, the mean fluorescence lifetime of normal tissue is lesser than that of cancer. The error bars in the figure are based on standard errors of mean.

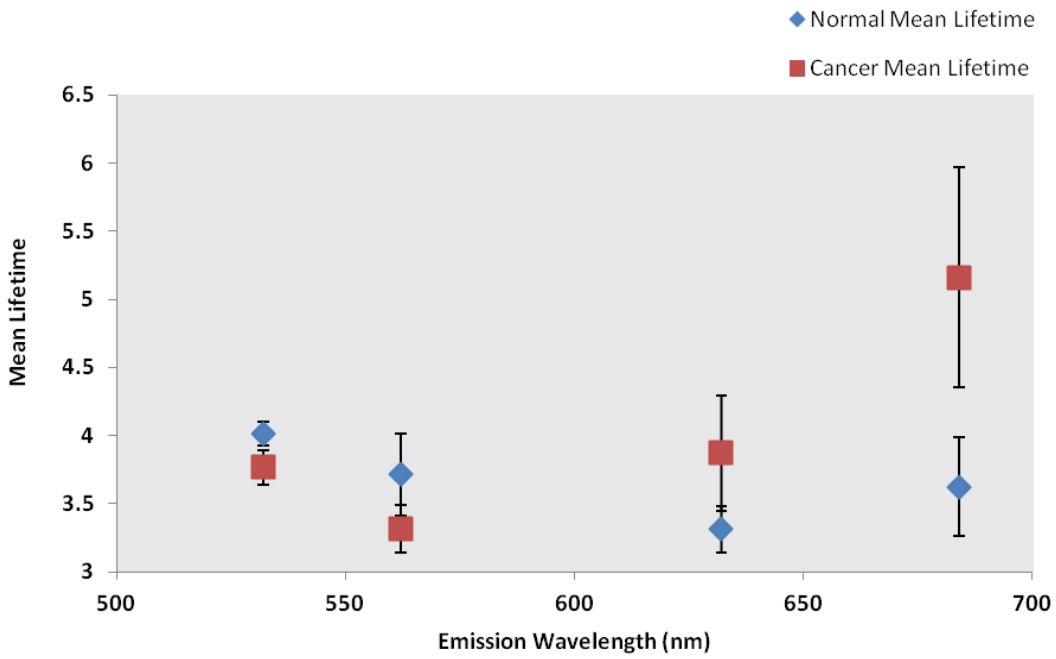

Fig 4.3: Comparison of Mean Fluorescence Lifetime between normal and cancer tissues.

A two-sample unequal variance test was performed between the normal and cancer mean lifetimes at each wavelength. The results indicate that confidence limits do encompass null hypothesis of a mean difference of zero, and that the p value in each of the wavelengths is greater ($p > 0.05$) than the stated confidence interval of 0.05.

Therefore, it can be concluded that there is enough evidence to accept the null hypothesis which says that there exists no significant difference of mean lifetime between cancer and normal tissue in case of all four wavelengths measured. Further, the weighted average lifetime $< \tau >$ is lower in normal tissue in comparison to malignant tissue at two wavelengths, 532 nm and 562 nm, which predominantly represents the changes in intrinsic fluorophores namely: Lipo-pigments and Flavins. However, the auto-fluorescence signal contribution at 632 nm and 684 nm, which is largely by Porphyrins, displays an opposite trend between the tissue types, normal and cancer.

To have a better insight into change in intinsic fluorescence between normal and malignant tissues, the individual fluorescence curvefit parameters namely, the fuorescence lifetimes τ_1 and τ_2 and their associated intensity components A_1 and A_2 were investigated. Global means over 7 samples were calculated for each of these parameters and compared with a two-sample ttest. Figs 4.4 (a) and 4.4 (b) show comparison between tissue types for intensity components A1 and A2 respectively. A two-sample t-test revealed significant differences at three wavelengths, namely: 562 nm, 632 nm and 684 nm. Only marginal difference was observed between normal and malignant breast tissues at wavelength 532 nm which had a p-value of 0.0507, thus not reaching the statistical significance.

Figs 4.5 (a) and 4.5 (b) show the comparison between tissue types for fluorescence lifetimes τ_1 and τ_2 respectively. A two sample t-test revealed significant difference in lifetime τ_2 at 684 nm. All other wavelengths for both τ_1 and τ_2 had a p value > 0.05, thus showing no significant difference between normal and cancer breast tissue. Error bars represent standard errors of mean . p-value less than 0.01 (99% confidence) are marked with a "★"

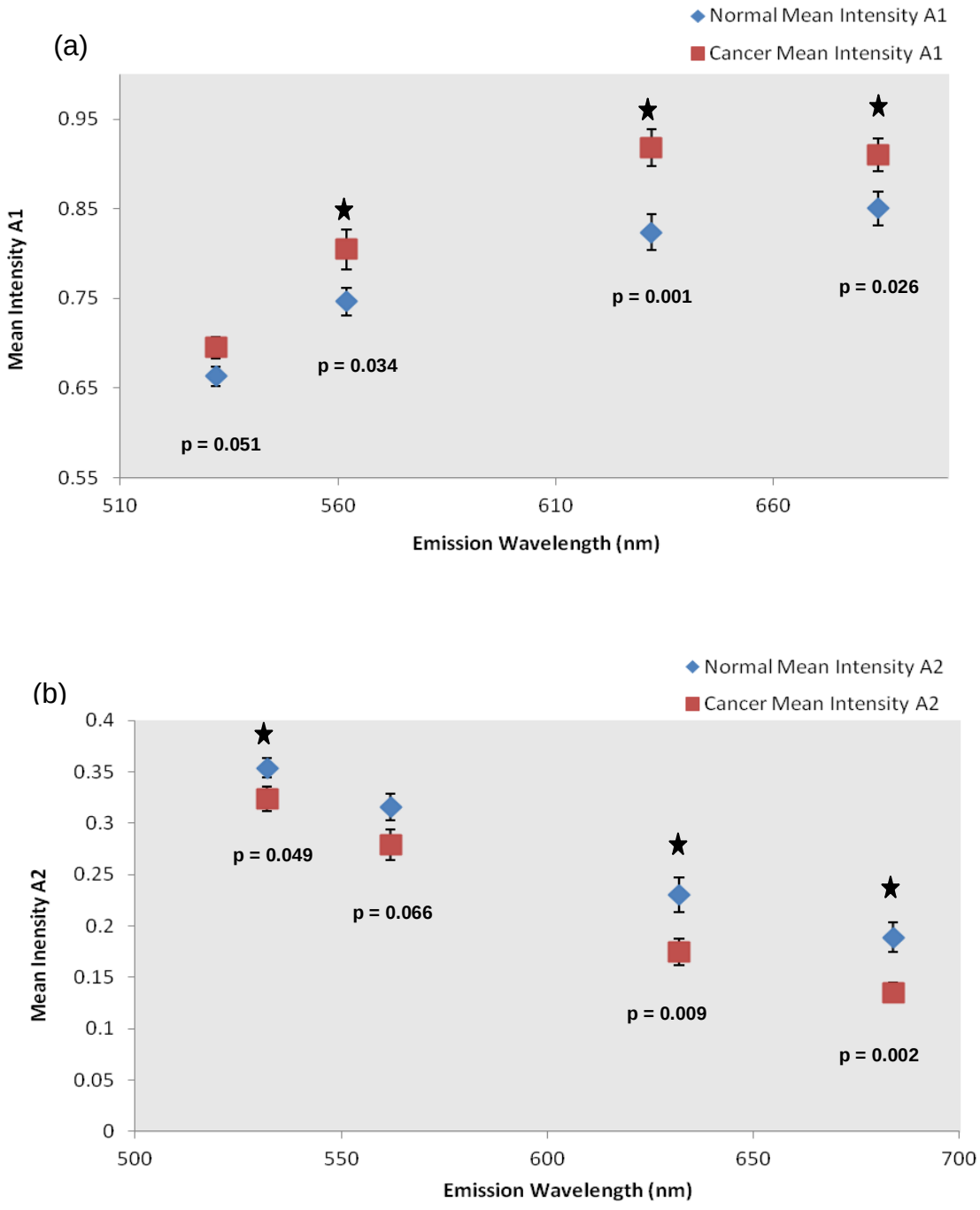

Fig 4.4: Comparison of global mean of (a) fluorescence intensities A_1 and (b) fluorescence intensities A_2 between normal and cancer breast tissues.

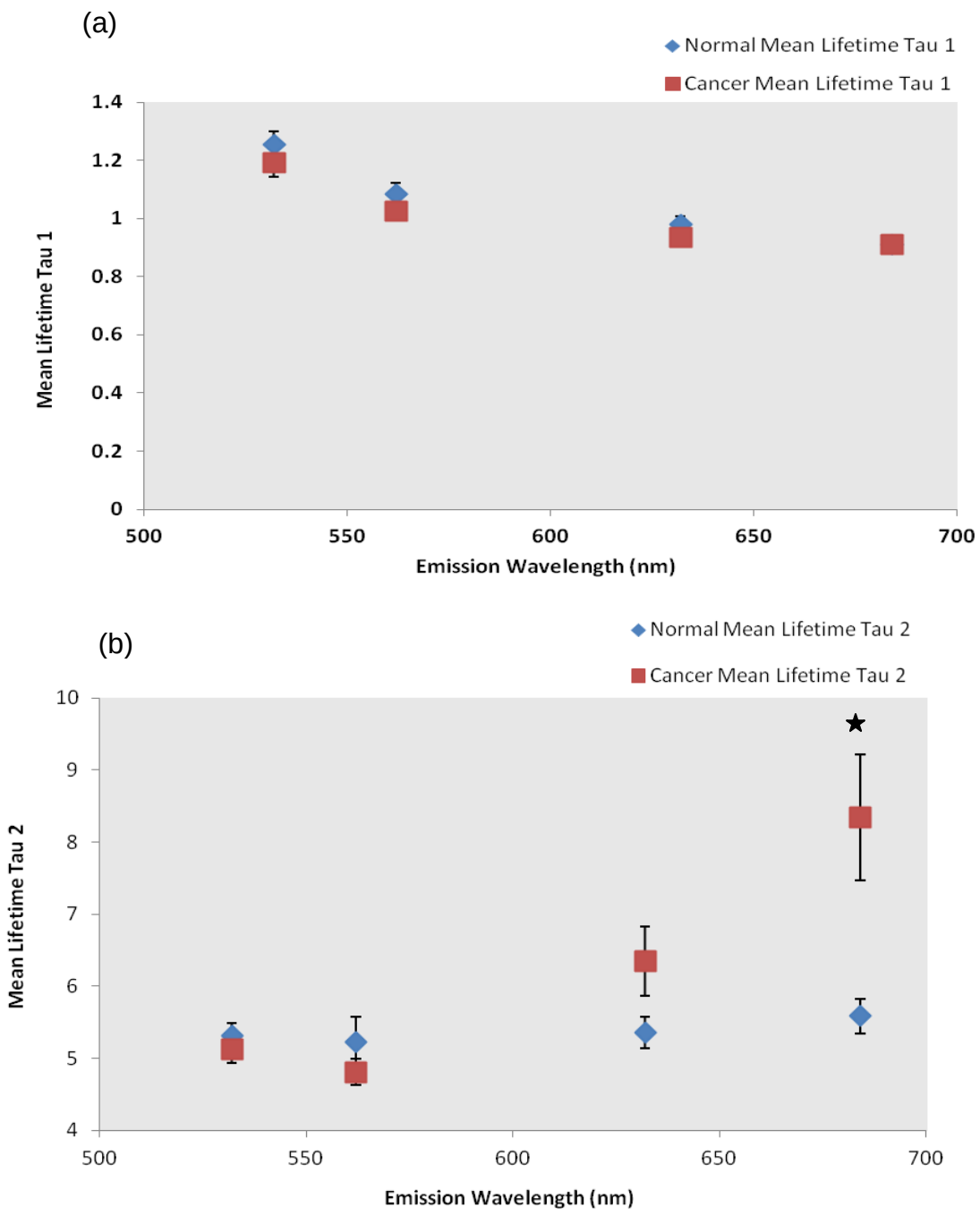

Fig 4.5: Comparison of global mean of (a) fluorescence lifetime τ_1 and (b) fluorescence lifetime τ_2 between normal and cancer breast tissues

The auto-fluorescence lifetime components can be recognized as (τ_1) being the short lifetime component spanning over the range of 1 - 1.2 ns, while (τ_2) being the long lifetime component ranging from 5 – 8 ns over the four wavelengths. (τ_1) and (τ_2) of the normal epithelium are predominantly lower compared to malignant tissues. Auto-fluorescence from Flavins and lipo-pigments from can be used to monitor alterations in cellular electron transport and protein metabolism. The corresponding lifetime amplitudes A1 and A2 also show a compensatory trend, with Mean Intensity A1 rising from 0.65 a.u. - 0.85 a.u. while Mean Intensity A2 dropping from 0.35 a.u - 0.15 a.u. Similar to (τ_1) and (τ_2), normal epithelium has lesser Mean Intensity A1 than cancer breast tissue. However, Mean Intensity A2 follows an opposite trend wherein normal tissue displays a higher Mean Intensity value than its counterpart cancer. It is interesting to note that the trend in average lifetime is largely contributed by the long lifetime component (τ_2). Difference in trend between the wavelengths [532 nm, 562 nm] and [632 nm, 684 nm] corresponding to shift in lifetimes can be attributed to tissue fluorescence from Flavins and porphyrins which suggest that the differences in spectra were caused by different environments in the two types of cells that make up the two tissue types.

With the auto-fluorescence lifetimes being complexly intertwined with their intensity components, using the significant parameters A1 and A2 for classification purposes have been erroneous. Further investigation is required to extrapolate these significant parameters and apply mixed linear regression model for generation of its Receiver Operation Characteristic Curve.

Fig 4.6 represents averaged reflectance spectra over 34 cancerous and 31 normal reflectance curves, respectively, all of which are normalized to the reference white light spectrum. As can be observed from the figure, the several dips found in the spectra of both tissue types represent

signatures of absorption by oxygenated and deoxygenated hemoglobin, which are major absorbers present in blood and have structured absorption bands spanning nearly the entire visible and near-infrared region.

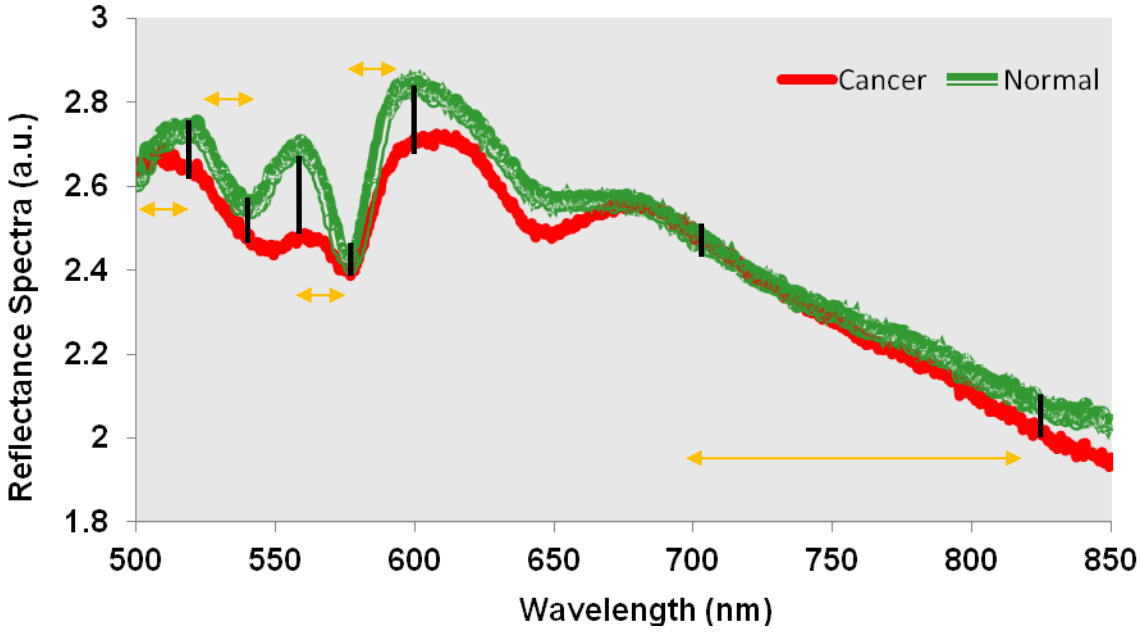

Fig 4.6: Comparison of Normalized Reflectance spectra between the normal and cancer breast tissues at six wavelength intervals.

Variation in [Hb] and [Hbo] between the two tissue types indicates state of tissue oxygenation while scattering coefficient throws light upon structural differences in the cellular morphology that makes up the normal and malignant breast tissue. It is well accepted that solid tumors are associated with decreased oxygen tension due to the increased oxygen demand of metabolically active cancer due to disordered and inefficient microvasculature created during the angiogenic process [65].

Table 4.1: Mean and Standard Errors of regression slope calculated for cancer and normal reflectance curves at six wavelength intervals.

Slope Interval (nm)	Cancer		Normal		p-value
	Mean (10^{-3})	Std Error (10^{-3})	Mean (10^{-3})	Std Error (10^{-3})	
500-525	0.47	0.14	-0.14	0.09	0.0013
525-540	-0.99	0.22	-0.84	0.13	0.59
540-560	0.88	0.15	0.05	0.10	9.34E-05
560-575	-1.97	0.19	-0.53	0.18	2.22E-06
575-590	2.82	0.34	1.81	0.19	0.017
700-800	-0.31	0.03	-0.37	0.02	0.17

Six wavelength intervals were chosen to calculate regression slopes of normal and cancer reflectance spectra to in order to quantitate the variation of [Hb] and [Hbo] that exhibit strong spectral signatures between 500 nm to 590 nm and the scattering coefficient between 700 nm to 850 nm. Table 4.1 lists these 6 spectral ranges and summarizes the mean and standard error of mean obtained over the six wavelength intervals. A two-sample t-test was performed on the slopes obtained from cancer and normal tissues, which revealed significant differences ($p < 0.05$) between cancer and normal tissue in four wavelength ranges, as observed in Table 4.1. As it can be observed here, the four wavelength intervals that show significance in slope variation lie between 500nm to 590 nm, bolstering the fact proved in previous studies owing to difference tissue oxygenation between normal and malignant tissues. Fig 4.7 shows regression slopes in four wavelength ranges selected from LRS (i.e., Fig. 4.6).

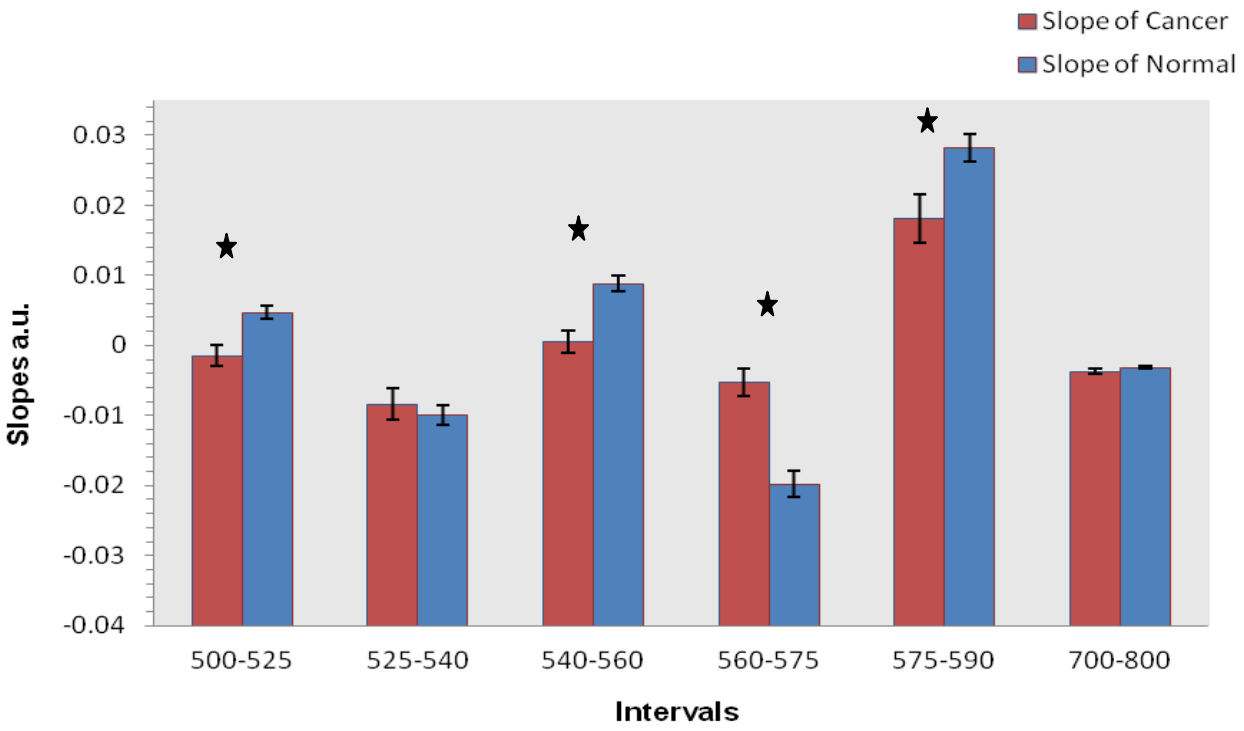

Fig 4.7: Comparison of Regression Slope from Reflectance spectra between the normal and cancer breast tissues

A mixed model linear regression analysis was performed on these four independent slope parameters for estimating ROC curve with repeated measure using GLMM as described in Section 4.2. Sensitivity and specificity were calculated and a ROC curve was generated, as shown in Fig. 4.8. This curve is a plot of sensitivity versus 1-specificity, where the sensitivity is defined as the probability that a test result is positive given the subject is truly diseased and the specificity is defined as the probability that the test result is negative given the subject is truly non-diseased.

ROC curve illustrates the trade-off between sensitivity and specificity by plotting true positive rate against the false positive rate for different possible thresholds used for a diagnostic test. This specific curve means that using the variation in regression slopes of the reflectance curves taken from invasive carcinoma and normal tissue, the two pathologically different samples can be differentiated with a sensitivity of 91.2% and specificity of 96.8%. The area under the ROC curve is 0.978 which determines the unconditional probability of correct ordering. Thus the LRS provides a positive predictive value of 91.2% and may accurately predict 31 out of 34 malignant spectra to be derived from Invasive Ductal Carcinoma.

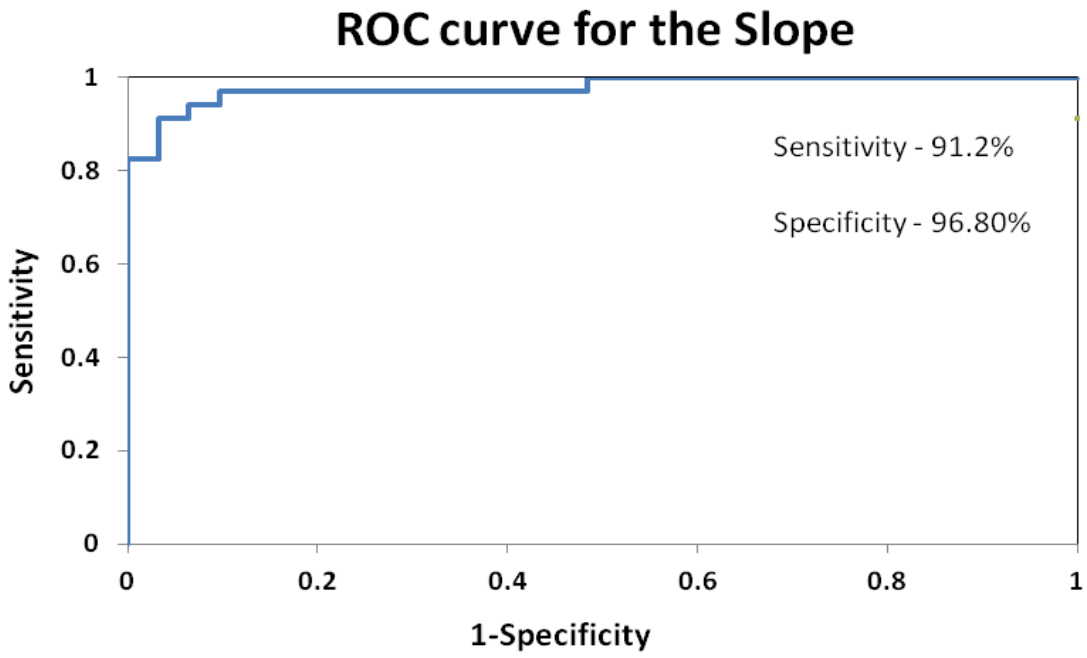

Fig 4.8: ROC curve generated for four slope parameters.

Histopathological confirmation was obtained from the samples used for optical studies. All of the cases used for above mentioned analysis were based on the findings of pathology verifying the regions to be cancer and normal tissues.

Fig 4.9 (a) is a histopathological illustration of Invasive Ductal Carcinoma that can be viewed in terms of physical, morphological, and pathological alteration of normal tissue: namely from a homogeneous stroma and two-layer epithelium structure as in Fig 4.9 (b) to a very heterogeneous stroma with enlargement of nuclei and increased micro-vascularization and scattering alterations as in Fig 4.9 (a). Histologically, IDC presents itself as cancerous cells that have invaded through the basement membrane into the surrounding stroma. These cancerous cells are also surrounded by a fibro-vascular matrix that displaces adipocytes.

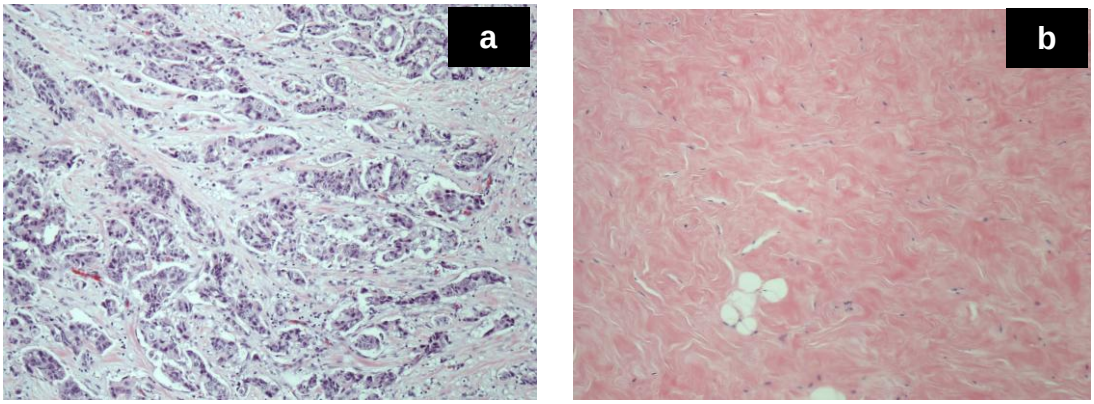

Fig 4.9: Histological findings showing difference between (a) Invasive Ductal Carcinoma and (b) Benign Breast stroma.

CHAPTER 5

CONCLUSION

This study shows the feasibility of using LRS and AFLM as independent techniques for differentiating cancer from normal tissue. Several optical parameters were obtained from the two techniques which could serve as potential biomarkers for identifying cancerous breast tissue. Results showed significant difference in amplitudes corresponding to auto-fluorescence decay lifetimes in AFLM whereas slopes of four distinct spectral regions were identified as contrast parameters in LRS for classifying cancer from non-cancerous tissue. AFLM measurements are highly sensitive to temperature, pH, oxygen content and nutrient supply of the measured tissue, while LRS is sensitive to changes in total blood concentration which is indicative of increased vasculature of tumor tissue as compared to normal tissue. The sensitivity and specificity of the two techniques are expected to be high due to their sensitivities to changes in the environment of the tissues.

In summary, significant differences have been noted in the auto-fluorescence properties of normal and malignant human breast tissues at four diagnostic wavelengths. In future studies it may be possible to build upon these findings in order to understand how the contribution of cellular fluorescence affects auto-fluorescence spectra measured in intact tissue. In depth investigation of workings of the targeted auto-fluorophores will help us understand the lifetime and the Mean intensity values extracted out of the data set. A meticulous algorithm to extrapolate significant parameters is necessary to successfully map the ROC curve for this imaging modality. Further, to investigate if there is need to use of all four wavelengths to serve

as contrast or to find a single wavelength that offers the best contrast in differentiating cancer from normal.

Specifically, LRS has proved to be a highly accurate technique with greater than 90% sensitivity and specificity. Given the low cost and simplicity of LRS, it could be a very promising tool for intra-operative detection of breast cancer positive margin detection. This observational study has shown that the patient demographics will be a major factor in maximizing the diagnostic capabilities of reflectance spectroscopy and auto-fluorescence lifetime measurements. Rigorous feature extraction algorithms are to be employed for picking out the best classifying parameters in case of AFLM to generate an ROC curve similar to that of LRS technique and to consider multi-class ROC generation for combining classifying parameters from both the modalities.

REFERENCES

1. M. Cutler. “Trans-illumination of the breast”. Surg. Gynecol. Obstet. 48, 721–727 (1929).
2. Cotran R.D et.al Robbins Pathologic Basis of Disease. 6th Ed., Philadelphia, W.B.Saunders Company (1999).
3. Burkitt H.G et.al. Wheater’s Basic Histopathology. 3rd Ed., Newyork, Churchill Livingstone (1996).
4. Stenberg SS. Histopathology for Pathologists. Philadelphia, Lippinncott-Raven.
5. Khan SA. et.al.” Phyllodes tumors of the Breast”. Current Treat Options. Oncol 2(2):139-147.
6. S. C. Lester, et al. “The breast.” In Pathologic Basis of Disease pages 1093–1119. W. B. Saunders, 1999.
7. WHO. World Health Organization Histological Typing of Breast Tumors, 2nd edn. Geneva: WHO, 1981.
8. A. Jemal, et.al. ”Cancer statistics”, 2010. CA: A Cancer Journal for Clinicians, 2010.
9. Kelsey JL, et.al. “Epidemiology of breast cancer”. Epidemiology Rev 1990, 12: 228-240.
10. A. C. Society, "Cancer Facts and Figs 2010," Atlanta: American Cancer Society, 2009.
11. Edwards BK et.al.” Annual report to the nation on the status of cancer, 1973-1999, featuring implications of age and aging on U.S. cancer burden”. Cancer 2002, 94 (10): 2766-2792.
12. S. W. Fletcher. “Breast cancer screening among women in their forties: an overview of the issues.” J. Natl. Cancer Inst. (22), 5–9, 1997.
13. K. Kerlikowske, et al. “Risk of breast cancer based on age and mammographic interpretation [see comments]. JAMA 276(1), 39 - 43, 1996.
14. Helmrich SP et.al “Risk factors for breast cancer” Am J Epidemiol 1983, 117 (1): 35-45.65

15. Claus EB et.al “Family history of breast and ovarian cancer and the risk of breast carcinoma in situ”. Breast Cancer Res Treat 2003, 78 (1): 7-15.
16. Henderson BE, Ross RK, Bernstein L. Estrogens as a cause of human cancer: the Richard and Hinda Rosenthal Foundation Award Lecture. Cancer Res 1988, 48: 246–253.
17. Brown P, Allen AR. Obesity linked to some forms of cancer. W V Med J 2002, 98 (6): 271-272.
18. Preston DL et.al. “Radiation effects on breast cancer risk: a pooled analysis of eight cohorts”. Radiat Res 2002, 158 (2): 220-235.
19. Stephens FO. “Breast cancer: aetiological factors and associations (a possible protective role of phytoestrogens)”. Aust N Z J Surg 1997, 67 (11): 755-760.
20. Atkinson HG. “Alcohol’s "darker side." A drink a day may raise a woman's risk of breast cancer”. Health News 2003, 9 (1): 4.
21. Chen WY et.al. “Use of postmenopausal hormones, alcohol, and risk for invasive breast cancer”. Ann Intern Med 2002, 137 (10): 798-804.
22. Donnegan et.al “Cancer of the Breast”. Philadelphia, W.B Saunders Company, 1995.
23. Dahnert. W “Radiology Review Manual”, 4th Ed, Baltimore, Williams and Wilkins, 1999, 449-474.
24. R. L. Birdwell, et al. “Mammographic characteristics of 115 missed cancers later detected with screening mammography and the potential utility of computer-aided detection.” Radiology 219(1), 192–202, 2001.
25. Gordon P.B et.al “Ultrasound for Breast Cancer screening and Staging”. Radiol Clin North Am, 2002, 40:431-441.
26. Boetes. C et.al. ” Breast tumors: comparative accuracy of MR imaging relative to mammography and us for demonstrating extent.” Radiology 197, 743–747, 1995.

27. B.Brooksby, et al. “Magnetic resonance-guided near-infrared tomography of the breast.” Rev. Sci. Instrum. 75(12), 5262–5270, 2004.
28. Ronald L. Bauer et.al. “Ductal carcinoma in situ-associated nipple discharge: A clinical marker for locally extensive disease”, Annals of Surg Onc, 452-455, 1998.
29. Pisano E.D et.al “Rate of Insufficient samples for Fine-Needle Aspiration for Non-palpable Breast lesions in a multicenter clinical trial”. Cancer 82: 679-688, 1998.
30. Liberman L et.al. “Stereotaxic 14-gauge Breast Biopsy – How many core biopsy specimens are needed.” Radiology 192(3): 793-795, 1994.
31. Ollila D.B et al “Breast Cancer Sentinel Node metastases: Histopathological Detection and Clinical Significance”. Cancer Control 8(5): 407-414, 2001.
32. Papatestas and Lesnick, “Treatment of the Breast with Modified Radical Mastectomy “. Surg Gynecol Obstet 140(1): 22-26, 1975.
33. Ragaz J et al. “Adjuvant Radiotherapy and Chemotherapy in Node Positive Pre-Menopausal Women with Breast Cancer”. N Engl J Med, 337(14): 956-962, 1997.
34. Eifel P et.al. “National Institute of Health Consensus Development Conference Statement: Adjuvant therapy for Breast Cancer”, J Natl Canc Insti, 93:979, 2001.
35. Fletcher G et.al. “Local results of Irradiation in the Primary Management of Localized Breast Cancer”. Cancer, 29:545, 1972.
36. Website of Stetson University: wgrubbs@stetson.edu
37. Gupta PK, et.al, “Breast cancer diagnosis using N2 Laser excited auto fluorescence spectroscopy “, Lasers Surg Med 21:417- 422, 1997.
38. Majumdar SK, et.al. “UV excited Auto-Fluorescence spectroscopy of Human Breast tissues for discriminating Cancerous tissue from benign tumor and Normal tissue”. Lasers Life Sci 00: 1-16, 1998.
39. HC van de Hulst. “Light Scattering by Small Particles.” 1957.

40. C.F. Bohren, et.al. ” Absorption and scattering of light by small particles.” Wiley New York, 1983.
41. Muller MG, et.al. “A Reflectance spectrofluorimeter for Real time spectral diagnosis of Disease”. Rev Sci Instrum 73(11): 3933-3937, 2002.
42. R. Richards-Kortum, et.al. “Quantitative optical spectroscopy for tissue diagnosis.” Annual Review of Physical Chemistry, 47(1):555{606, 1996.
43. K. Sokolov, et.al. “Reflectance spectroscopy with polarized light: is it sensitive to cellular and nuclear morphology.” Optics Express, 5(13):302{317, 1999.
44. N. Ramanujam. “Fluorescence spectroscopy of neoplastic and non-neoplastic tissues Neoplasia”, 2(1/2):89{117, 2000.
45. Chih-Wen Kan, et.al. ” Applications in Optical Spectroscopy for Cancer Detection and Diagnosis”, chapter 2, pages 27{50.Springer, 2008.
46. Website of Jobin Yvon, Inc, 2004
47. O'Connor, D. V.; Phillips, D. Time-correlated Single Photon Counting, Academic Press: 1984.
48. Website of Ocean Optics : http://oceanoptics.com
49. D.M. Jameson and T.L. Hazlett, “Biophysical and Biochemical Aspects of Fluorescence Spectroscopy”, Plenum Press, New York, pp. 105–133, 1991.
50. Becker, W., et.al. “Fluorescence lifetime images and correlation spectra obtained by multidimensional TCSPC.” Proc. SPIE 5700, 144–151, 2005.
51. D. Arier, et.al. “Reflectance spectroscopy for diagnosis of epithelial pre-cancer: model-based analysis of fiber-optic probe designs to resolve spectral information from epithelium and stroma.” Applied Optics, 44(20):4291{4305, 2005.
52. www.virtualmedicalcenter.com
53. http:/medlib.med.utah.edu/Webpath

54. http://history.nih.gov/exhibits/genetics/sect2.htm
55. http://www.cme-usa.com/usprobes.aspx
56. http://ultrasound-image.blogspot.com/2010/01/ultrasound-contrast-agents.html
57. www.medrayimaging.com
58. http://www.shsu.edu/~chm_tgc/chemilumdir/JABLONSKI.html
59. www.icms.qmul.ac.uk
60. www.andor.com
61. www.m-scale.com
62. O'Connor, D. V.; Phillips, D. Time-correlated Single Photon Counting, Academic Press: 1984
63. www.beamq.com
64. Stephen.D.Kachman “An introduction to Generalized Linear Mixed Models” Department of biometry, University of Nebraska–Lincoln.
65. Vaupel P et.al “Oxygen status of malignant tumors: pathogenesis of hypoxia and significance for tumor therapy.” Semin Oncol 2001; 28:29–35.
66. Cubeddu, R., et.al. “Time-resolved fluorescence imaging in biology and medicine.” Phys. D Appl. Phys. 35, R61–R76, 2002.
67. Georgakoudi, et.al. “Fluorescence, reflectance, and light-scattering spectroscopy for evaluating dysplasia in patients with Barrett’s esophagus.” Gastroenterology, 120(7):1620-1629, 2001.
68. Georgakoudi, et.al. “Trimodal spectroscopy for the Detection and characterization of Cervical Pre-cancers in-vivo”, Am J Obstet Gynecol 186(3): 374-382, 2002.
69. Palmer GM, et.al., “Optimal methods for Fluorescence and Diffuse Reflectance Measurements of Tissue Biopsy Samples”, Lasers in Surgery and Medicine 30(3): 191-200, 2002

70. I.J. Bigio, et.al. ”Diagnosis of breast cancer using elastic-scattering spectroscopy: preliminary clinical results.” Journal of Biomedical Optics, 5:221, 2000.
71. D.C.G. de Veld, et.al.” Clinical study for classification of benign, dysplastic, and malignant oral lesions using auto-fluorescence spectroscopy.” Journal of Biomedical Optics, 9(5):940-950, 2004.
72. N. Ramanujam, et.al. “Spectroscopic diagnosis of cervical intraepithelial neoplasia in vivo using laser-induced fluorescence spectra at multiple excitation wavelengths.” Lasers in Surgery and Medicine, 19(1):63-74, 1996.
73. EN Atkinson, et.al. “Statistical techniques for diagnosing cancer using fluorescence spectroscopy.”, J Cell Biochem Suppl, 23:25-30, 1995.
74. D.C.G. de Veld, et.al. ”Auto-fluorescence and diffuse reflectance spectroscopy for oral oncology.” Lasers in Surgery and Medicine, 36(5):356-364, 2005.
75. Changfang Zhu, et.al. ” Diagnosis of breast cancer using fluorescence and diffuse reflectance spectroscopy: a monte-carlo-model-based approach. “, Journal of Biomedical Optics, 13(3):034015, 2008.
76. H. Liu, et.al. "Near-Infrared Spectroscopy and Imaging of Tumor Vascular Oxygenation," Methods in Enzymology, vol. 386, pp. 349-378, 2004.
77. K. Bensalah, et.al. “Optical Reflectance Spectroscopy to Differentiate Benign and from Malignant Renal Tumors at Surgery,” J. of Urology 73(1), 178-181, 2009.
78. H. Liu, et.al. "Near infrared and visible spectroscopic measurements to detect changes in light scattering and hemoglobin oxygen saturation from rat spinal cord during peripheral stimulation," Neuro-image 40(1), 217-227, 2008.

BIOGRAPHICAL INFORMATION

Shivaranjani Shivalingaiah was born on the 18th of May, 1987 in Bangalore, India. She received her Bachelor of Engineering degree in Biomedical Engineering from Vishveshwaraiah Technological University, India in June 2009. During this tenure she did her six months internship at Sagar Apollo hospital in Bangalore. In August 2009 she enrolled in graduate school in the Department of Biomedical Engineering, a Joint program of Biomedical Engineering at the University of Texas at Arlington and University of Texas at Southwestern Medical Center at Dallas and completing the same in August 2011. During her graduate studies she worked on Positive margin detection of Breast cancer.